scientific reports

Check for updates

OPEN

# Inhibition of galanin receptor 3 slows down retina degeneration in retinitis pigmentosa through modulation of inflammatory and oxidative stress response

Maria Azam[1], Zaiddodine Pashandi[1], Mingda Liu[1] & Beata Jastrzebska[1,2]✉

**Photoreceptors require a finely regulated balance of oxygen, nutrients, and waste removal to sustain visual function. In inherited retinopathies like rhodopsin (RHO)-associated retinitis pigmentosa (RP), disruption in retinal homeostasis leads to neurodegeneration. The most common mutation in RHO, P23H, causes protein misfolding, endoplasmic reticulum (ER) stress, and activation of inflammatory and oxidative stress pathways, ultimately leading to photoreceptor death. Upregulation of the NLRP3 inflammasome and NF-κB signaling in RHO mutant models, highlight inflammation as a key contributor to disease progression, yet targeted therapies remain limited. G protein-coupled receptor (GPCR) signaling is a crucial regulator of retinal homeostasis. We identified galanin receptor 3 (GALR3), a GPCR expressed in retinal cells, as a mediator of photoreceptor degeneration. In the *Rho*$^{P23H/+}$ mouse model, GALR3 expression was upregulated in response to the mutation-induced chronic stress. Both genetic ablation and pharmacological inhibition of GALR3 with the selective antagonist SNAP-37,889 attenuated photoreceptor loss and improved retinal survival. Mechanistically, GALR3 inhibition suppressed pro-inflammatory signaling, promoted anti-inflammatory responses, and activated antioxidant defense pathways. These findings reveal GALR3 as a critical mediator of inflammatory and oxidative stress responses in RHO P23H-associated RP, and its inhibition offers a promising therapeutic strategy to slow retinal degeneration and preserve vision in inherited retinopathies.**

**Keywords** Galanin receptors, Neuroinflammation, Oxidative stress, Photoreceptor, Retinal degeneration, Retinitis pigmentosa

The photoreceptor cells in the retina absorb photons, convert their energy into electrical signals, and route the signal to the brain[1]. An adequate supply of oxygen and nutrients, as well as the timely removal of toxic metabolites, is required to sustain retinal health and proper visual function[2]. To maintain retinal homeostasis, all processes occurring in the retina must be rigorously controlled. Modulation of G protein-coupled receptor (GPCR) signaling, including adrenergic receptors, serotonin receptors, adrenoreceptors, and other neuroprotective GPCRs, plays a crucial neuroprotective role against transient pathological insults[3–8]. However, the exact implications of this signaling modulation in retinal homeostasis are poorly understood. Even less is known about the effect of GPCR signaling modulation in inherited retina pathologies. The visual GPCR rhodopsin (RHO) is the most abundant protein in rod photoreceptors and serves as both a key structural component and the primary initiator of phototransduction[9,10]. The misfolding mutations in RHO cause an overload of newly synthesized protein within the endoplasmic reticulum (ER), which causes an imbalance of retinal homeostasis, leading to progressive vision loss in retinitis pigmentosa (RP)[11,12]. The most common RHO mutation, P23H, accounts for 10–12% of autosomal dominant RP (adRP) cases in the United States, and currently, no cure is available[13]. The activation of multiple cell death pathways by a genetic mutation, including ER stress response, inflammatory response, oxidative stress response, and caspase-dependent and independent programmed cell death, are the obstacles counteracting the satisfactory progress of developing effective treatment strategies for RP[12,14]. Along with the upregulation of the ER stress markers, significant upregulation of proinflammatory markers has been

[1]Department of Pharmacology, School of Medicine, Case Western Reserve University, 10900 Euclid Ave, Cleveland, OH 44106-4965, USA. [2]Cleveland Center for Membrane and Structural Biology, School of Medicine, Case Western Reserve University, 10900 Euclid Ave, Cleveland, OH 44106, USA. ✉email: bxj27@case.edu

found in the RHO mutant-related mouse models, including *Rho*$^{P23H/+}$ *knock-in* mice[15–17]. Inflammation is an ancient component of innate immunity[18,19], activated by pathogens or cellular by-products. These stimuli trigger the upregulation of Nod-like receptor 3 (NLRP3) in the retina, either via activation of the nuclear factor κB (NF-κB) pathway through Toll-like receptor or by reactive oxygen species (ROS) produced in the retina under stress[20–22]. NLRP3 forms a multiprotein complex with apoptosis-associated ASC adaptor protein and caspase-1 that is involved in the maturation and secretion of proinflammatory cytokines, including IL-1β and IL-18[17,23,24]. Previous work suggests that the genetic ablation of either NLRP3 or NF-kB, or pharmacological inhibition of NF-kB signaling, suppresses apoptotic processes and exerts neuroprotective effects in models of retinal degeneration[25–29]. Although data suggest that both NLRP3 and NF-κB could be considered therapeutic targets, no FDA-approved therapy targeting these markers is yet available.

As mentioned earlier, various biological processes that occur in the complex retinal tissue must be tightly regulated to maintain homeostasis[2]. Imbalanced homeostasis harms photoreceptor cells and compromises the integrity of the blood-retina barrier (BRB)[30–32]. GPCR signaling plays a key regulatory role in this process[3–8]. As we recently found, the galanin receptor 3 (GALR3), which is expressed in various retinal cells, including retinal pigment epithelium (RPE), inner segments of photoreceptors, retinal neurons within the inner nuclear layer, and ganglion cells[7,33], plays a pivotal role in retina degeneration, and inhibition of its signaling either with the specific SNAP-37,889 antagonist[34] or by genetic depletion of the receptor provides a neuroprotective effect in mouse models of light-induced retinal degeneration[33]. Of note, natural ligands of GALR3, galanin and spexin were found in similar retinal compartments[35,36]. Interestingly, GALR3-mediated signaling has been implicated in the regulation of inflammatory processes in various diseases, including neuroinflammation[37–41].

In this study, we investigated the neuroprotective mechanism associated with the inhibition of GALR3 signaling in *Rho*$^{P23H/+}$ *knock-in* mice, a well-established model of RP. We observed that GALR3 expression is upregulated in response to chronic stress induced by the RHO P23H mutation, mirroring the response seen following bright light exposure[33]. Notably, genetic ablation or pharmacological inhibition of GALR3 in *Rho*$^{P23H/+}$ mice attenuated photoreceptor degeneration. This protective effect was accompanied by downregulation of the NF-κB –NLRP3 axis and a shift in the retinal immune response, characterized by reduced expression of pro-inflammatory markers and increased expression of anti-inflammatory markers. Additionally, GALR3 inhibition promoted the activation of antioxidant defense pathways, which collectively preserved the integrity of the BRB and contributed to photoreceptor survival.

Altogether, this work suggests that GALR3 signaling contributes to retinal pathology in RP, where upregulated proinflammatory signaling accelerates the degenerative phenotype of RHO P23H-mediated RP. Notably, modulation of GALR3 signaling attenuates these processes and delays retinal degeneration in this retinopathy and thus represents a promising therapeutic avenue to preserve vision in RP.

## Results

### Inhibition of GALR3 signaling slows down photoreceptor cell death in RP

We recently showed that GALR3 is upregulated in retinas following light exposure in bright light-sensitive mouse models, and that both genetic depletion and pharmacological inhibition of GALR3 protect against photoreceptor loss[33]. These results suggested that GALR3 may also contribute to chronic retinal degeneration, such as RP. Indeed, our initial study in heterozygous *Rho*$^{P23H/+}$ mice confirmed that a blockade of GALR3 signaling partially rescued photoreceptors in these mice[33]. Thus, in this follow-up study, we investigated the role of GALR3 in RP, the therapeutic potential of its inhibition, and the underlying mechanism of photoreceptor protection in more detail.

To examine the expression levels of GALR3, we first performed RT-qPCR analyses and found that at postnatal day 33 (P33), *Galr3* mRNA levels, along with the mRNA expression of its endogenous agonist *spexin*, were significantly increased in *Rho*$^{P23H/+}$ mice in both the retina and eyecup compared with wild-type (WT) controls (Fig. 1a-c), and resembled changes observed in light-damaged retinas[33]. Consistently, elevated GALR3 protein levels were observed in immunolabeled retinal cryosections of *Rho*$^{P23H/+}$ mice (Fig. 1d-e). As reported previously, photoreceptor degeneration in *Rho*$^{P23H/+}$ mice becomes noticeable around P15, with shortened inner and outer segments compared to age-matched WT controls, followed by a rapid phase of degeneration between P15 and P33 that continues thereafter[15,42]. To evaluate the protective potential of GALR3 inhibition longitudinally, *Rho*$^{P23H/+}$ mice were treated every other day with the selective GALR3 antagonist SNAP-37,889[34] for two or four weeks from P21 to P33 or P45, followed by evaluation of retinal morphology and function. In parallel, the impact of genetic depletion of *Galr3* was evaluated at the same time points. Age-matched WT mice were used as controls. Consistent with previous observation, our in vivo optical coherence tomography (OCT) imaging and histological analyses revealed that the outer nuclear layer (ONL) thickness was reduced by ~ 50% in *Rho*$^{P23H/+}$ mice relative to WT controls at P33 (Fig. 2a-d). Importantly, attenuation of GALR3 signaling led to a ~ 25% increase in the ONL thickness at P33 and ~ 16% at P45 compared to untreated *Rho*$^{P23H/+}$ mice, indicating a partial preservation of photoreceptor cells. While the GALR3 inhibition did not completely halt degeneration, it slowed its progression. Furthermore, levels of key markers of photoreceptor structure and function, such as RHO and M-cone opsin, were elevated at both the mRNA and protein levels in SNAP-37,889-treated and *Galr3* knockout *Rho*$^{P23H/+}$ mice compared with untreated controls (Fig. 2e-g and Fig. S1). Remarkably, genetic deletion of *Galr3* appeared more effective than pharmacological inhibition, suggesting a stronger or more sustained suppression of the deleterious signaling cascade. In addition, the electroretinography (ERG) responses were enhanced in both *Rho*$^{P23H/+}$*Galr3*$^{-/-}$ and SNAP-37,889-treated *Rho*$^{P23H/+}$ mice compared to non-treated mice at both P33 and P45 (Fig. 3). Thus, these findings support the unrecognized role of GALR3 in promoting photoreceptor degeneration and highlight GALR3 inhibition as a potential therapeutic strategy to enhance photoreceptor survival in inherited retinal diseases.

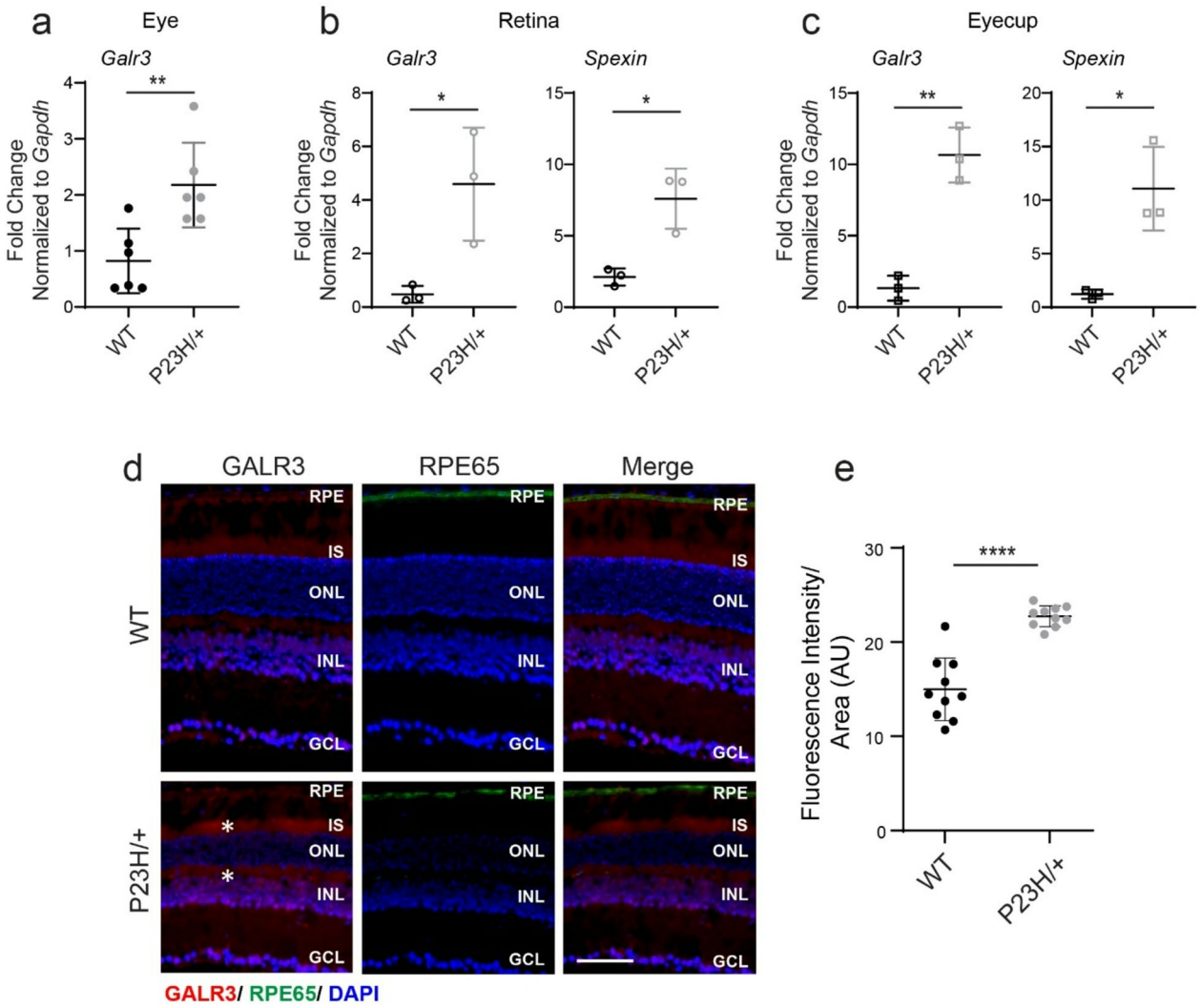


**Fig. 1**. The expression of GALR3 and spexin in mouse eyes. **a-c** mRNA expression levels of *Galr3* and *spexin* in the whole eye, retina, and eyecup of *Rho*$^{P23H/+}$ and WT mice detected with RT-qPCR. **d** GALR3 immunoreactivity (red) detected in retinal cryosections of *Rho*$^{P23H/+}$ and WT mice. RPE cells were detected with an antibody recognizing RPE65 protein (green). Nuclei were stained with DAPI (blue). Stars indicate regions with enhanced GALR3 expression. Scale bar, 50 µm. *RPE* retinyl pigment epithelium, *IS* inner segments, *ONL* outer nuclear layer, *INL* inner nuclear layer, *GCL* ganglion cell layer. **e** Quantification of GALR3 expression as a mean of red fluorescence intensity detected in retinal cryosections stained with anti-GALR3 antibody. Error bars represent standard deviation (S.D.). Statistically significant changes that were calculated with Student's t-test are shown with asterisks, $*P<0.05$; $**P<0.01$; $***P<0.001$; $****P<0.0001$. P23H/+, *Rho*$^{P23H/+}$.

## Inhibition of GALR3 signaling attenuates the levels of inflammatory markers in RP

Müller glia and microglia are key components of the retinal innate immune system that play critical roles in responding to neurodegenerative stress[18,19]. Müller glia extend radially across the retina, with their processes spanning from the inner limiting membrane to the outer limiting membrane and are among the first responders to photoreceptor injury[43,44]. Upon sensing photoreceptor degeneration, Müller cells initiate a reactive gliosis program characterized by upregulation of glial fibrillary acidic protein (GFAP) and secretion of signaling molecules that activate resident microglia, which then migrate to the outer retina to clear dying photoreceptors and maintain retinal health[2,45]. However, in the context of sustained insults due to inherited mutations, this inflammatory response often becomes dysregulated, exacerbating retinal degeneration[46].

Given the role of GALR3 in the regulation of inflammatory responses, we investigated whether the inhibition of GALR3-mediated signaling, either pharmacologically or through genetic depletion, could attenuate retinal inflammation associated with degenerative processes driven by inherited mutations such as the P23H mutation in RHO. Consistent with a reactive gliosis response, GFAP expression was markedly upregulated in Müller glia of *Rho*$^{P23H/+}$ mice at both P33 and P45 compared to WT controls. Notably, blockade of GALR3 signaling significantly attenuated GFAP expression at both time points (Fig. 4a-b, upper panel, Fig. 4c–d, and Fig. S2),

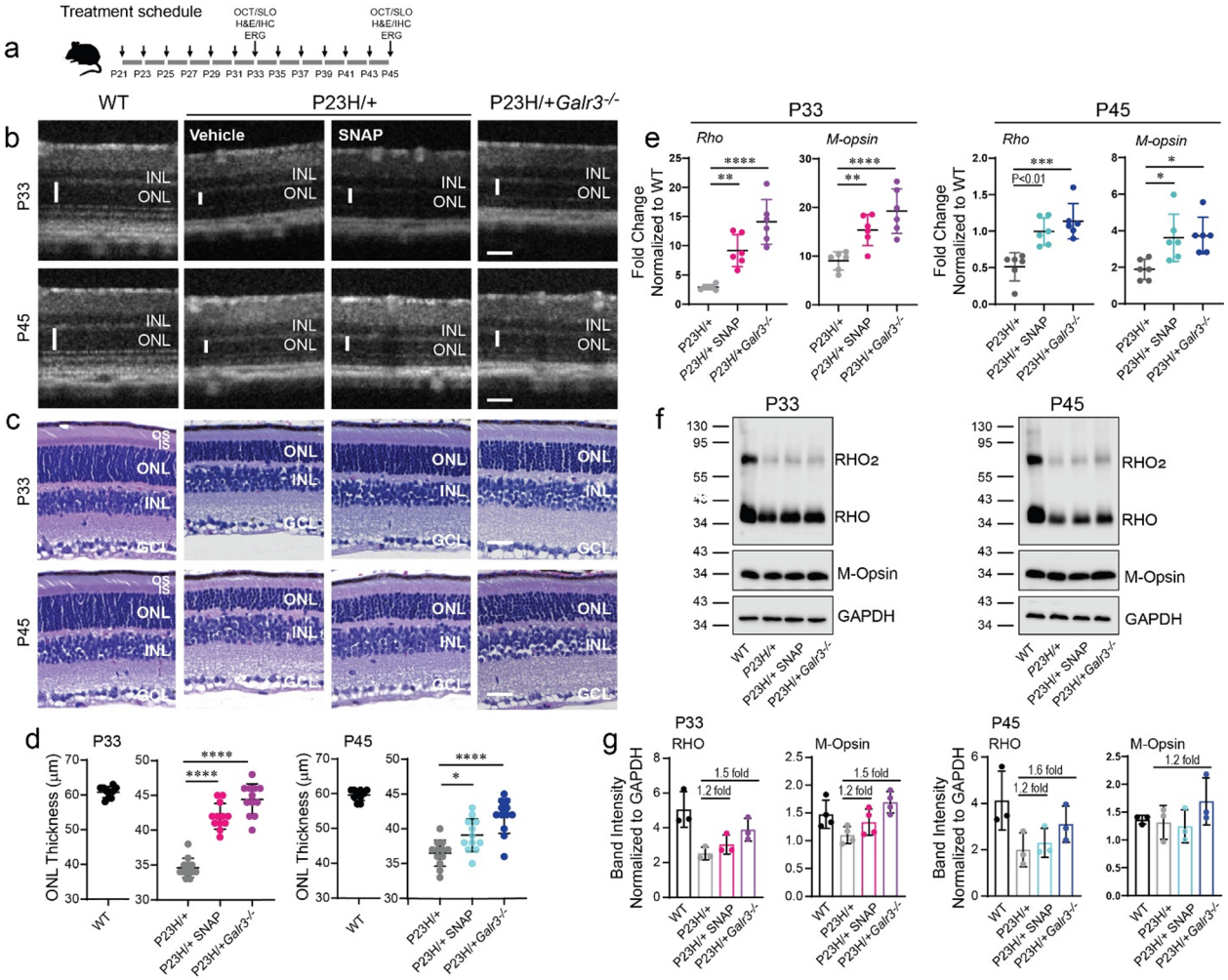


**Fig. 2**. Effects of GALR3 inhibition on retinal morphology and the expression of structural proteins in *Rho*$^{P23H/+}$ mice. The analyses were performed in WT, *Rho*$^{P23H/+}$, antagonist-treated *Rho*$^{P23H/+}$, and *Rho*$^{P23H/+}$*Galr3*$^{-/-}$ mice at postnatal day 33 (P33) and P45. **a** Schematic of mouse treatment regimen with SNAP-37,889 antagonist. **b** The representative OCT images of the retina. Scale bar, 100 μm. **c** The representative histological retinal images stained with H&E. Scale bar, 50 μm. **d** Quantification of the outer nuclear layer (ONL) thickness at 500 mm from the optic nerve head (ONH). **e** mRNA expression levels of *Rho* and *M-opsin* detected with RT-qPCR. **f** Protein expression levels of RHO and M-Opsin assessed by immunoblotting. The representative immunoblots are shown. Full immunoblots are shown in Supplementary Information in Fig. S1. **g** Quantification of protein bands intensities of RHO and M-Opsin detected in three independent immunoblot experiments, normalized to GAPDH. Error bars represent S.D. Statistical analysis was performed with one-way ANOVA and post hoc Turkey's tests. Statistically significant changes are shown with asterisks. *$P < 0.05$; **$P < 0.01$; ***$P < 0.001$; ****$P < 0.0001$. P23H/+, *Rho*$^{P23H/+}$; P23H/+ SNAP, *Rho*$^{P23H/+}$ treated with antagonist; P23H/+*Galr3*$^{-/-}$, *Rho*$^{P23H/+}$*Galr3*$^{-/-}$. *GCL* ganglion cell layer, *INL* inner nuclear layer, *IS* inner segments, *OS* outer segments.

suggesting a suppression of gliotic activation. In parallel, the number of activated microglia, identified by IBA-1 immunostaining on retinal cryosections and flat mounts, was significantly elevated in *Rho*$^{P23H/+}$ mice relative to WT. However, GALR3 inhibition, whether through administration of its antagonist SNAP-37,889 or by genetic depletion, led to a substantial reduction in IBA-1-positive microglia cells (Fig. 4a–b, lower panel and Fig. 4e–f, and Figs. S3 and S4). These findings indicate that suppression of GALR3 signaling dampens both Müller glia and microglial activation, thereby reducing the inflammatory milieu associated with inherited retinal degeneration.

## Inhibition of GALR3 signaling inhibits the expression of proinflammatory cytokines in RP

During the onset of retinal inflammation, microglia shift from a homeostatic (M0) state to a pro-inflammatory (M1) phenotype in response to pathological stimuli[47–49]. This transition is characterized by activation of the NF-κB signaling cascade, which promotes the transcription and secretion of pro-inflammatory cytokines and chemokines, including interleukin-6 (IL-6) and interleukin-18 (IL-18). NF-κB activation also induces expression of NLRP3, a key component of the inflammasome complex. Upon activation, the NLRP3 inflammasome

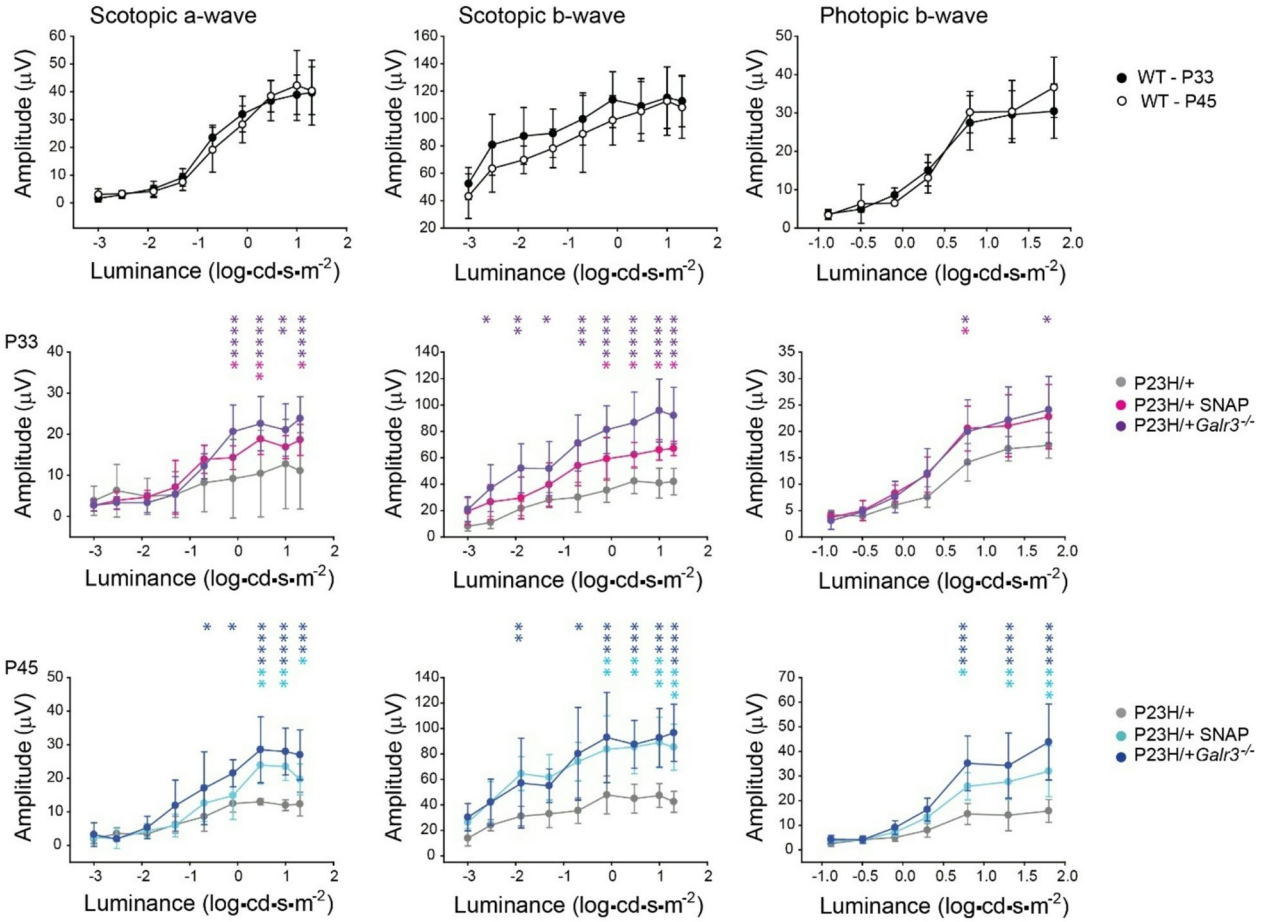


**Fig. 3**. Effects of GALR3 inhibition on retinal function in *Rho*$^{P23H/+}$ mice. Retinal function was assessed with electroretinography (ERG) recordings in WT, *Rho*$^{P23H/+}$, antagonist-treated *Rho*$^{P23H/+}$, and *Rho*$^{P23H/+}$*Galr3*$^{-/-}$ mice at P33 and P45. Error bars represent S.D. Statistical analysis was performed with two-way ANOVA and post hoc Turkey's tests. Statistically significant changes are shown with asterisks. *$P<0.05$; **$P<0.01$; ***$P<0.001$; ****$P<0.0001$. P23H/+, *Rho*$^{P23H/+}$; P23H/+ SNAP, *Rho*$^{P23H/+}$ treated with antagonist; P23H/+*Galr3*$^{-/-}$, *Rho*$^{P23H/+}$*Galr3*$^{-/-}$.

initiates caspase-1 activation, leading to the processing of pro-IL-1β and pro-IL-18 into their mature, bioactive forms, thereby amplifying the inflammatory response. In retinas affected by RP, the transcription of IL-1β, IL-18, and NLRP3 is further stimulated by increased levels of ROS, which act as secondary triggers of inflammation. Concurrently, other pro-inflammatory mediators such as CXCL chemokines, tumor necrosis factor-alpha (TNF-α), and neuronal nitric oxide synthase (nNOS) are also upregulated, contributing to the chronic inflammatory environment. Interestingly, although the expression of GALR3 was not detectable in resting M0 macrophages, its levels were shown to increase upon M1 polarization, suggesting GALR3's role in promoting proinflammatory responses[41].

In this study, we investigated whether the inhibition of GALR3 signaling could attenuate this pathological inflammatory cascade in *Rho*$^{P23H/+}$ mice. Using RT-qPCR, immunoblotting, and immunohistochemistry (IHC), we found that expression levels of NF-κB and NLRP3 were significantly elevated in *Rho*$^{P23H/+}$ retinas, but were markedly reduced upon GALR3 inhibition, either pharmacologically or through genetic depletion (Fig. 5a–d, Fig. S5a, and Fig. S6). Similarly, while pro-caspase-1 levels were increased in *Rho*$^{P23H/+}$ mice, cleaved (active) caspase-1 was only detected in untreated mice and was absent in GALR3-inhibited conditions (Fig. 5b, 5e and Fig. S7), suggesting suppression of inflammasome activation. Significant upregulation of these inflammatory markers was observed at P33, whereas changes at P45 were notably reduced (not shown), suggesting that the initiation of the inflammatory response occurs early in the course of retinal degeneration in RP. Furthermore, RT-qPCR analysis confirmed that GALR3 inhibition significantly reduced the expression of key pro-inflammatory markers , including IL-6, IL-18, TNF-α, CXCLs, and nNOS, at both P33 and P45 (Fig. 6a and Fig. S5 b). These results highlight the anti-inflammatory effect of GALR3 inhibition and support its potential as a therapeutic strategy for mitigating chronic inflammation and preserving photoreceptor integrity in inherited retinal degenerative diseases.

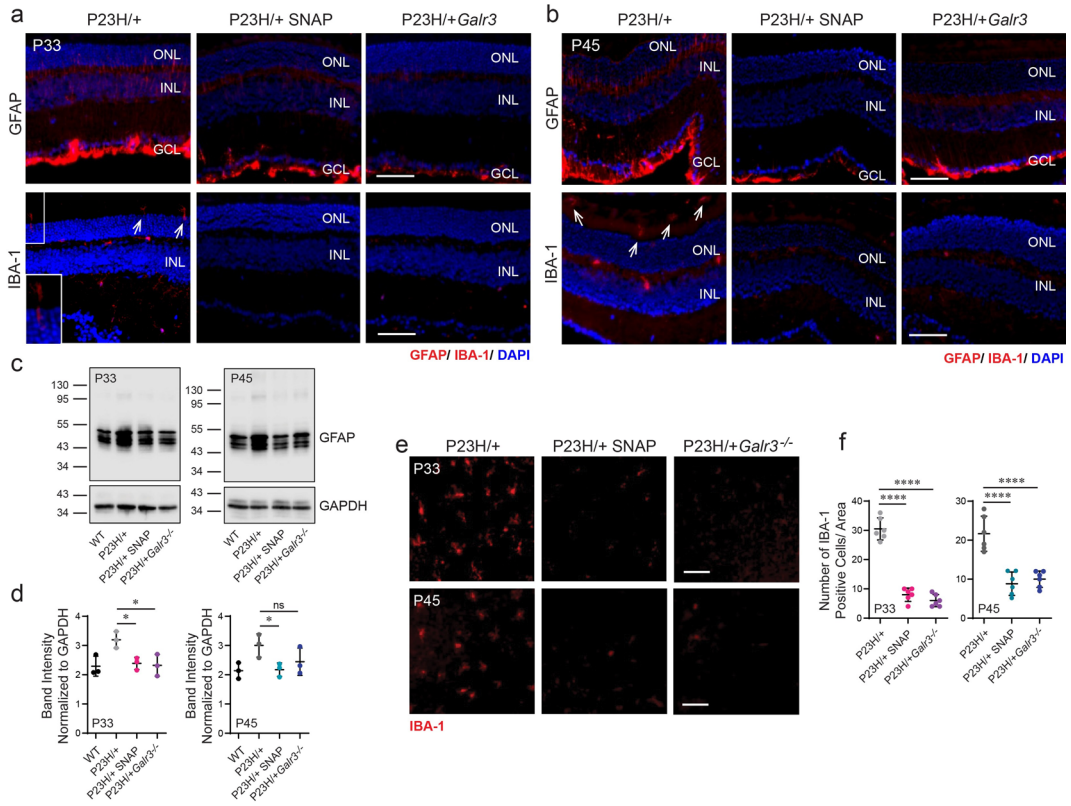


**Fig. 4**. Effects of GALR3 inhibition on retinal inflammation in *Rho*$^{P23H/+}$ mice. The analyses were performed in WT, *Rho*$^{P23H/+}$, antagonist-treated *Rho*$^{P23H/+}$, and *Rho*$^{P23H/+}$*Galr3*$^{-/-}$ mice at postnatal day 33 (P33) and P45. **a** Detection of GFAP expression (red) (upper panel) and IBA-1 expression (red) (lower panel) in retinal cryosections at P33. Arrows indicate IBA-1-positive immune cells migrating to the outer retina. Detection of GFAP expression (red) (upper panel) and IBA-1 expression (red) (lower panel) in retinal cryosections at P45. Arrows indicate IBA-1-positive immune cells migrating to the outer retina (enlarged images are shown in Fig. S3). Nuclei were stained with DAPI (blue). Scale bar, 50 µm. Detection of GFAP and IBA-1 in retinal cryosections of WT mice is shown in Fig. S4. **c** Protein expression levels of GFAP in mouse eyes assessed by immunoblotting at P33 and P45. Full immunoblots are shown in Supplementary Information (Fig. S2). **d** Quantification of protein bands intensities of GFAP detected in three independent immunoblot experiments, normalized to GAPDH. **e** Detection of IBA-1 positive cells (red) in retinal flat mounts at P33 and P45. **f** Quantification of IBA-1 positive cells in retinal flat mounts. Error bars represent S.D. Statistical analysis was performed with one-way ANOVA and post hoc Turkey's tests. Statistically significant changes are shown with asterisks. *$P<0.05$; **$P<0.01$; ***$P<0.001$; ****$P<0.0001$; *ns* not statistically significant. P23H/+, *Rho*$^{P23H/+}$; P23H/+ SNAP, *Rho*$^{P23H/+}$ treated with antagonist; P23H/+*Galr3*$^{-/-}$, *Rho*$^{P23H/+}$*Galr3*$^{-/-}$. *GCL* ganglion cell layer, *INL* inner nuclear layer, *ONL* outer nuclear layer.

## Inhibition of GALR3 signaling activates anti-inflammatory responses

To determine if attenuation of pro-inflammatory signaling coincides with activation of anti-inflammatory responses upon GALR3 signaling inhibition, we screened for several characteristic markers. Microglia at the M2 phenotype induce upregulation of anti-inflammatory cytokines, including IL-10, and promote tissue restoration. Indeed, the expression of IL-10 was elevated in *Rho*$^{P23H/+}$ mice treated with SNAP-37,998 as well as in mice with genetically depleted *Galr3* compared to non-treated *Rho*$^{P23H/+}$ mice. In addition, collagen-1 A, peroxisome proliferator-activated receptor gamma (PPARγ), and transforming growth factor-beta 1 (TGF-β1) are often upregulated during tissue repair processes. Levels of these markers were elevated in SNAP-37,998-treated *Rho*$^{P23H/+}$ mice and *Rho*$^{P23H/+}$*Galr3*$^{-/-}$ mice as compared to non-treated *Rho*$^{P23H/+}$ mice at P33 (Fig. 6b). However, by P45 the levels of these markers were comparable across all groups, suggesting that inflammatory responses equilibrate at later stages. Together these findings demonstrate that negative modulation of GALR3 signaling shifts the balance from pro-inflammatory to anti-inflammatory processes, thereby attenuating inflammation in retinas under chronic stress induced by the inherited P23H mutation in RHO.

## Inhibition of GALR3 signaling enhances the oxidative stress defense responses

In RP, inflammatory processes are triggered by both ER stress and mitochondrial dysfunction, the latter contributing to the excessive production of ROS[12,14]. Activated microglia further exacerbate retinal degeneration by releasing matrix-degrading proteases and increasing ROS production. Thus, inflammation and oxidative stress are tightly interconnected, with oxidative stress often preceding and amplifying inflammatory responses.

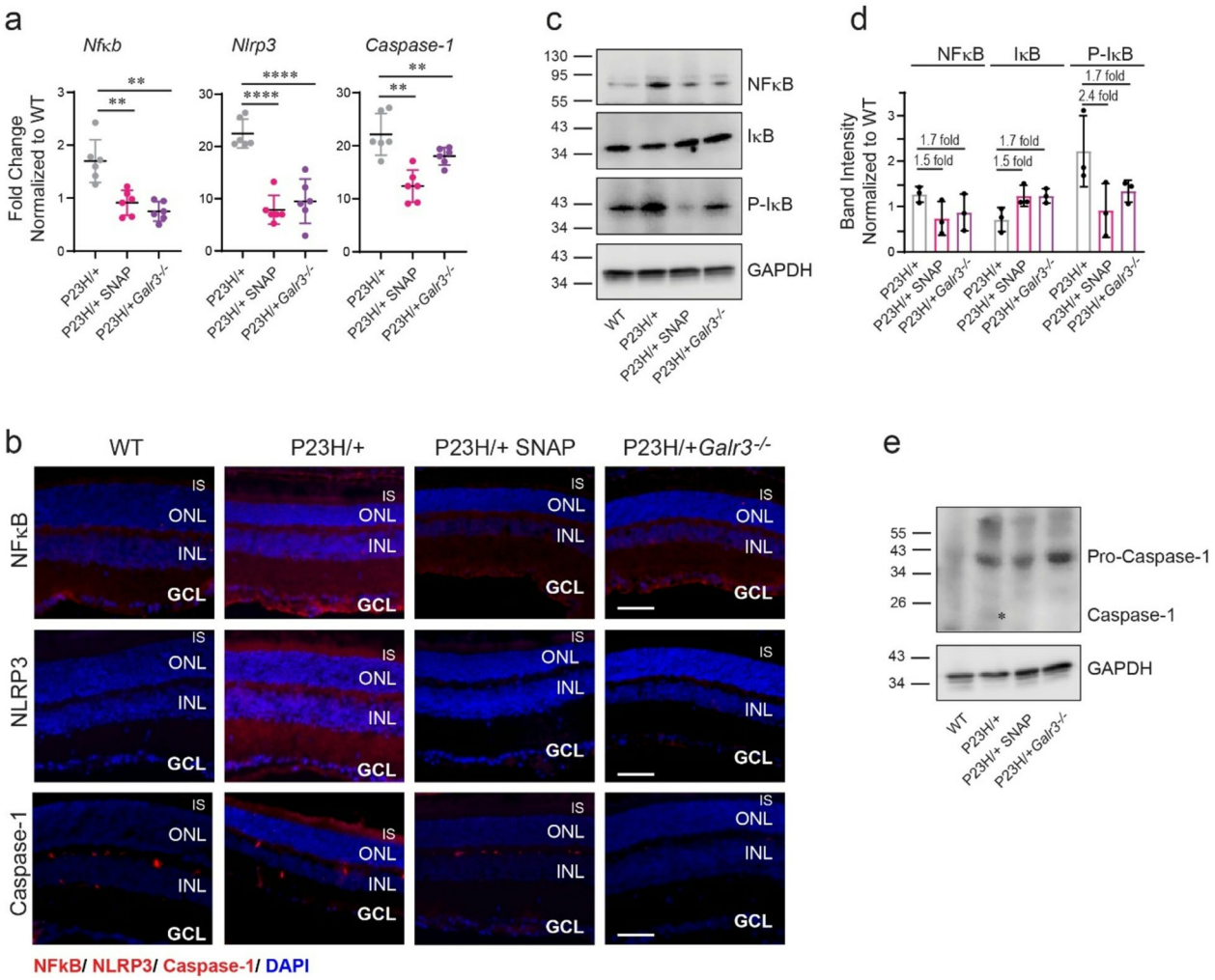


**Fig. 5**. Effects of GALR3 inhibition on NF-κB signaling in the eyes of *Rho*$^{P23H/+}$ mice. The analyses were performed in WT, *Rho*$^{P23H/+}$, antagonist-treated *Rho*$^{P23H/+}$, and *Rho*$^{P23H/+}$*Galr3*$^{-/-}$ mice at P33. **a** mRNA expression levels of *Nf-κb*, *Nlrp3*, and *Caspase-1* detected with RT-qPCR. **b** Immunofluorescence detection of NF-κB signaling components, including NF-κB, NLRP3, and Caspase-1 (red) in cryosections. Nuclei were stained with DAPI (blue). Scale bar, 50 µm. **c** Protein expression analysis of NF-κB signaling, including NF-κB, total IκB, and phosphorylated IκB (P-IκB) detected by immunoblotting. Full immunoblots are shown in Supplementary Information (Fig. S6). **d** Quantification of protein bands intensities of NF-κB, IκB, and P-IκB detected from three independent immunoblot experiments, normalized to GAPDH. Fold change was calculated. Error bars represent S.D. **e** Detection of pro-Caspase-1 and cleaved (activated) Caspase-1 in retinal protein extracts by immunoblotting. Full immunoblots are shown in Supplementary Information (Fig. S7). Error bars represent S.D. Statistical analysis was performed with one-way ANOVA and post hoc Turkey's tests. Statistically significant changes are shown with asterisks. *$P<0.05$; **$P<0.01$; ***$P<0.001$; ****$P<0.0001$. P23H/+, *Rho*$^{P23H/+}$; P23H/+ SNAP, *Rho*$^{P23H/+}$ treated with antagonist; P23H/+*Galr3*$^{-/-}$, *Rho*$^{P23H/+}$*Galr3*$^{-/-}$.

Under normal physiological conditions, nuclear factor erythroid 2–related factor 2 (NRF2) plays a central role in maintaining redox homeostasis by limiting NF-κB activation and upregulating antioxidant and detoxifying enzymes, including heme oxygenase-1 (HMOX-1), superoxide dismutase (SOD), glutathione peroxidase 4 (GPx4), as well as glutamate cysteine ligase (GCL), which is essential for glutathione (GSH) synthesis. However, under pathological conditions, chronic NF-κB activation can suppress NRF2 signaling, reducing the expression of these protective enzymes. Notably, NRF2 can also be positively regulated by anti-inflammatory cytokines[50–52].

In this study, we found that the suppression of GALR3 signaling attenuates NF-κB activation. Therefore, we further examined whether GALR3 inhibition influences the NRF2 pathway and its downstream antioxidant targets. In *Rho*$^{P23H/+}$ mice genetically lacking *Galr3*, we observed a significant upregulation of *Nrf2* mRNA expression at both P33 and P45, along with increased mRNA levels of antioxidant enzymes including *Sod1*, *Sod2*, *Gpx4*, *Hmox-1*, and *catalase* (Fig. 7a and Fig. S5c). A similar, though less pronounced, effect was seen in *Rho*$^{P23H/+}$ mice treated with the GALR3 antagonist SNAP-37,998. Immunoblot analysis confirmed elevated protein levels of catalase and catalytic subunit of GCL (GCLc) (Fig. 7b-c and Fig. S8). These findings suggest that

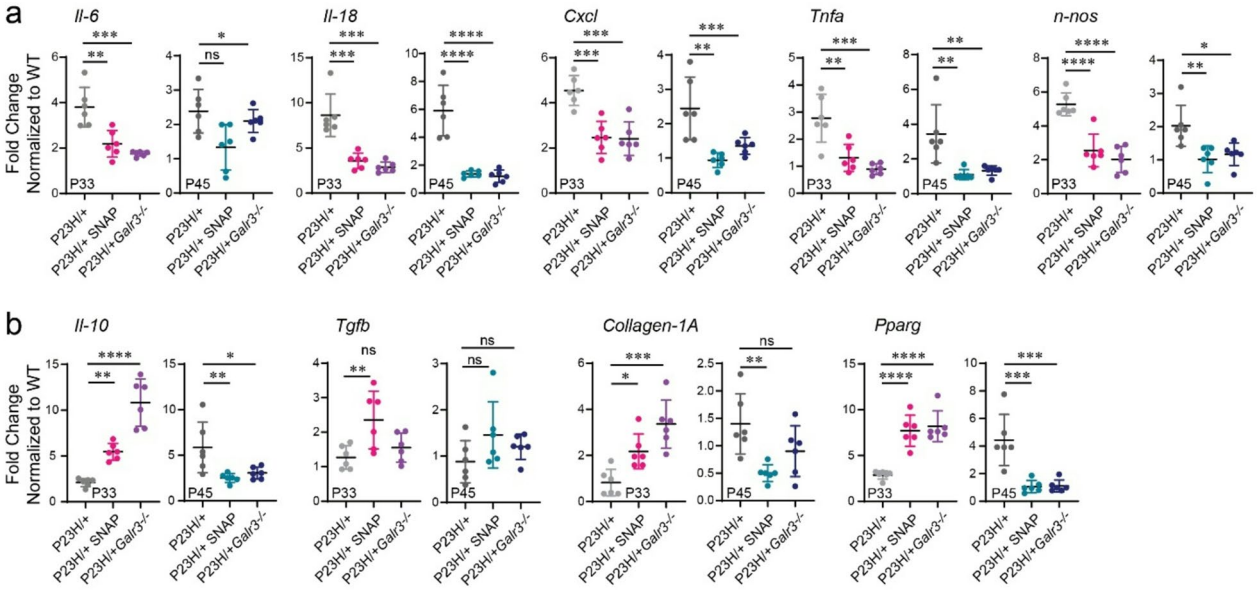


**Fig. 6**. Effects of GALR3 inhibition on the expression of pro-inflammatory and anti-inflammatory markers in the eyes of $Rho^{P23H/+}$ mice. The analyses were performed in WT, $Rho^{P23H/+}$, antagonist-treated $Rho^{P23H/+}$, and $Rho^{P23H/+}Galr3^{-/-}$ mice at P33 and P45. **a** mRNA expression levels of pro-inflammatory cytokines detected with RT-qPCR. **b** mRNA expression levels of anti-inflammatory markers detected with RT-qPCR. Error bars represent S.D. Statistical analysis was performed with one-way ANOVA and post hoc Turkey's tests. Statistically significant changes are shown with asterisks. $^{*}P<0.05$; $^{**}P<0.01$; $^{***}P<0.001$; $^{****}P<0.0001$; ns, not statistically significant. P23H/+, $Rho^{P23H/+}$; P23H/+ SNAP, $Rho^{P23H/+}$ treated with antagonist; P23H/+$Galr3^{-/-}$, $Rho^{P23H/+}Galr3^{-/-}$.

GALR3 inhibition enhances the NRF2-mediated antioxidant response, particularly at the early to mid-stage of degeneration, thereby mitigating oxidative stress and reducing inflammation in photoreceptors. This mechanism may contribute to the protective effects observed in GALR3-deficient or antagonist-treated RP models.

## Inhibition of GALR3 signaling preserves BRB integrity in RP

RPE cells, a key component of the BRB, are essential for maintaining retinal integrity and supporting photoreceptor metabolism[53]. In turn, photoreceptor outer segments serve as a major energy source for RPE cells, highlighting the interdependence of these two cell types. The inner BRB is formed by retinal capillary endothelial cells and relies on the proper organization of tight junctions to maintain retinal homeostasis[54]. Photoreceptor degeneration, as seen in RP, disrupts this balance and can lead to disorganization of tight junctions, thereby compromising the integrity and function of both outer and inner BRBs[49,55]. Infiltration of pro-inflammatory microglia into the outer retina further exacerbates this disruption[56].

Disintegration of BRB in mouse models of RP was reported previously[49]. To evaluate this phenomenon in our mouse models, we examined tight junction integrity at P33 and P45. In WT mice retinas, RPE cells displayed a regular hexagonal morphology with intact cell-cell junctions, as visualized by immunodetection of zonula occludens-1 (ZO-1), a tight junction adaptor protein. In contrast, ~ 7% of RPE cells in $Rho^{P23H/+}$ mice at P33 showed loss of cell-cell contacts, with these disruptions becoming more pronounced at P45 (Fig. 8a-b). Remarkably, both genetic ablation and pharmacological inhibition of GALR3 markedly reduced these structural abnormalities, preserving RPE monolayer integrity.

To further evaluate the functional consequences of BRB disruption, we assessed its permeability. Commonly used methods include FITC-dextran perfusion, FITC-albumin perfusion, or FITC-conjugated anti-albumin immunostaining on retinal flat mounts to detect leakage of circulating plasma proteins. In our study, we employed a well-established anti-albumin-FITC immunostaining approach[57–60]. Under physiological conditions, albumin is confined within the vasculature, however, when the BRB is compromised, albumin extravasates into the retinal tissue. Consistent with this, in WT retinas, fluorescence was largely restricted to blood vessels, whereas in $Rho^{P23H/+}$ mice, substantial extravascular albumin was detectable at both P33 and P45 (Fig. 8c-d), indicating impaired vascular barrier function. In contrast, GALR3-deficient mice and those treated with the GALR3 antagonist displayed markedly reduced albumin leakage, demonstrating preserved capillary integrity.

Together, these findings demonstrate that GALR3 signaling contributes to BRB breakdown in RP. The inhibition of this pathway, either genetically or pharmacologically, helps maintain both structural and functional integrity of the BRB, highlighting GALR3 as a potential therapeutic target for preserving retinal barrier function in degenerative retinal diseases.

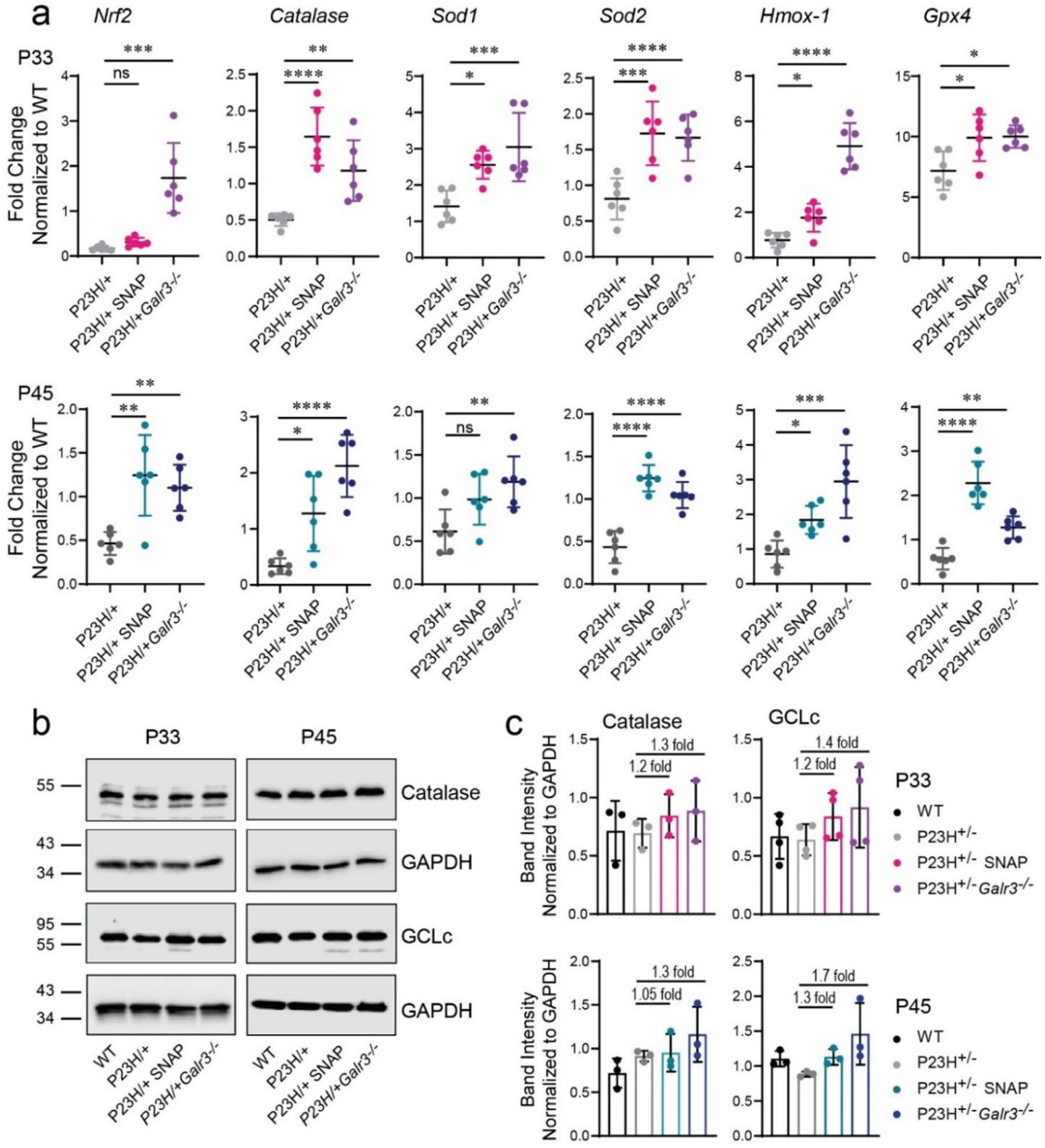


**Fig. 7**. Effects of GALR3 inhibition on oxidative stress in the eyes of *Rho*$^{P23H/+}$ mice. The analyses were performed in the following groups of mice: WT, *Rho*$^{P23H/+}$, antagonist-treated *Rho*$^{P23H/+}$, and *Rho*$^{P23H/+}$*Galr3*$^{-/-}$ at P33 and P45. **a** mRNA expression levels of antioxidant markers detected with RT-qPCR. **b** Protein expression analysis of representative antioxidant enzymes, including catalase and GCLc, detected by immunoblotting. Full immunoblots are shown in Supplementary Information (Fig. S8). **c** Quantification of protein bands intensities of catalase and GCLc detected from three independent immunoblot experiments, normalized to GAPDH. Fold change was calculated. Error bars represent S.D. Statistical analysis was performed with one-way ANOVA and post hoc Turkey's tests. Statistically significant changes are shown with asterisks. *$P < 0.05$; **$P < 0.01$; ***$P < 0.001$; ****$P < 0.0001$; ns, not statistically significant. P23H/+, *Rho*$^{P23H/+}$; P23H/+ SNAP, *Rho*$^{P23H/+}$ treated with antagonist; P23H/+*Galr3*$^{-/-}$, *Rho*$^{P23H/+}$*Galr3*$^{-/-}$.

## Inhibition of GALR3 signaling suppresses inflammation-related neurotoxicity in photoreceptor cells in vitro

Photoreceptor loss is a central hallmark of retinal degeneration in RP, and neuroinflammation driven by pro-inflammatory microglia plays a significant role in exacerbating photoreceptor cell death. Lipopolysaccharide (LPS), a glycolipoprotein component of the bacterial cell wall, is widely used to induce a strong pro-inflammatory response in immune cells. To investigate whether inhibition of GALR3 signaling can mitigate microglia-induced neurotoxicity in photoreceptors, we utilized a cultured cell system involving the photoreceptor-derived 661 W

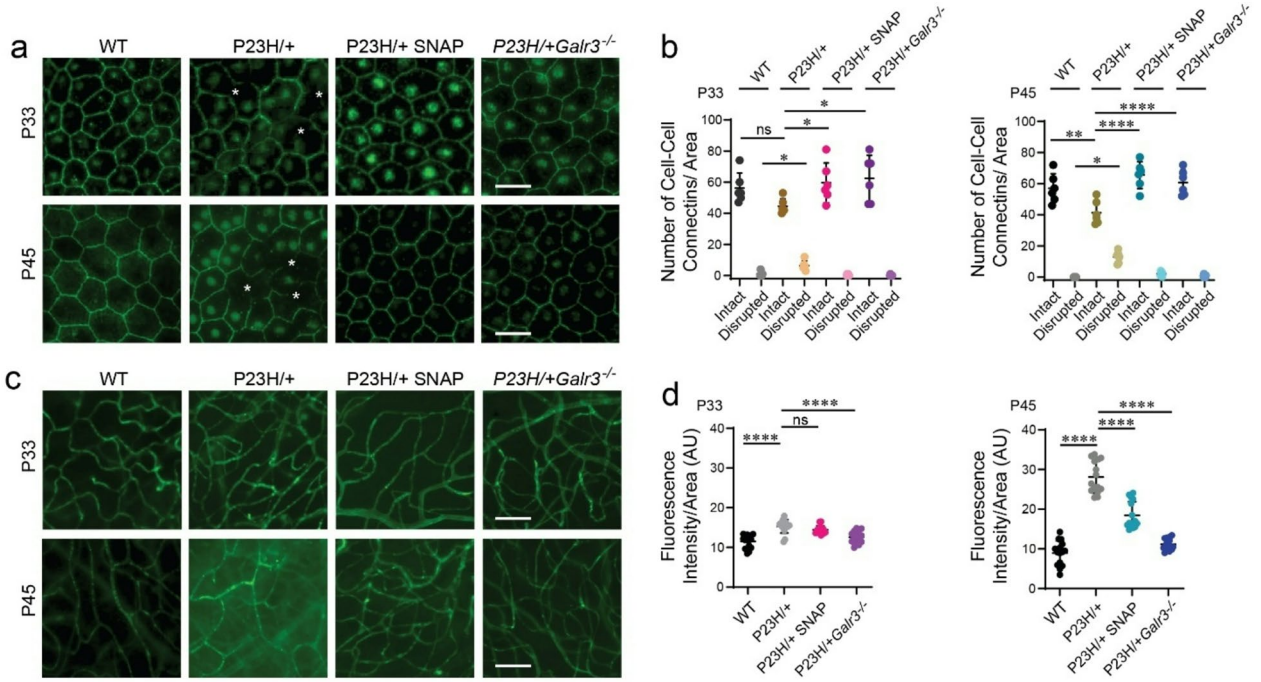


**Fig. 8**. Effects of GALR3 inhibition on BRB integrity in the eyes of *Rho*$^{P23H/+}$ mice. The analyses were performed in the following groups of mice: WT, *Rho*$^{P23H/+}$, antagonist-treated *Rho*$^{P23H/+}$, and *Rho*$^{P23H/+}$*Galr3*$^{-/-}$ at P33 and P45. **a** Immunofluorescence labeling of ZO-1 on RPE/choroidal flat mounts. **b** Quantification of RPE cell-cell connections per area. **c** Detection of albumin leakage on retinal flat mounts with anti-albumin antibody conjugated to fluorescein. **d** Quantification of fluorescence intensity in retinal tissue. Error bars represent S.D. Statistical analysis was performed with one-way ANOVA and post hoc Turkey's tests. Statistically significant changes are shown with asterisks. *$P<0.05$; **$P<0.01$; ***$P<0.001$; ****$P<0.0001$; ns, not statistically significant. P23H/+, *Rho*$^{P23H/+}$; P23H/+ SNAP, *Rho*$^{P23H/+}$ treated with antagonist; P23H/+*Galr3*$^{-/-}$, *Rho*$^{P23H/+}$*Galr3*$^{-/-}$.

cell line and conditioned media from LPS-activated BV-2 microglial cells (Fig. 9a). LPS-mediated activation of BV-2 cells was evidenced by upregulation of IL-6, TNF-α, and CXCL pro-inflammatory cytokines (Fig. 9b). 661 W cells were incubated with this inflammatory media for 24 and 48 h. Following treatment, we observed a significant upregulation of pro-inflammatory cytokines IL-6, TNF-α, and CXCL in 661 W cells compared to non-treated controls. In contrast, 661 W cells with GALR3 knockdown exhibited a markedly attenuated cytokine response, indicating that loss of GALR3 reduced the pro-inflammatory effects of microglial conditioned media (Fig. 9c).

These findings suggest that although activated microglia can exert neurotoxic effects on photoreceptors, GALR3 is a key mediator of this inflammatory response. Downregulation of GALR3 in photoreceptor-derived cells markedly reduced inflammatory cytokine expression, highlighting the central role of GALR3 signaling in modulating microglia-induced neuroinflammation in RP.

## Discussion

Retinal homeostasis is essential for sustaining vision but is often disrupted in degenerative eye diseases. Support cells such as the RPE, microglia, and Müller glia play key roles in maintaining this balance, with their function tightly regulated by GPCR signaling pathways[2,61,62]. However, under stress conditions, GPCR activation can exacerbate inflammatory responses, ultimately accelerating retinal degeneration[3–8]. Targeting GPCRs, including visual opsins[63–66] and other stress-responsive receptors, has shown promise in mitigating retinal damage[4,8]. Recently, we identified GALR3 as a novel modulator of retinal homeostasis[33]. In mouse models susceptible to acute light-induced retinal injury, GALR3 and its endogenous ligand spexin, were upregulated in response to bright light exposure. On the other hand, genetic depletion or pharmacological inhibition of GALR3 with its specific antagonist SNAP-37,889 significantly preserved photoreceptor viability. Extending these findings, in this study, we observed a similar upregulation of GALR3 and spexin in retinas of *Rho*$^{P23H/+}$ mouse model of adRP, further implicating GALR3 in chronic retinal degeneration. However, blocking GALR3 signaling enhanced photoreceptor survival at the early and mid-stages of the disease.

Although the mechanisms underlying photoreceptor loss in RP remain incompletely understood, hallmarks of RHO-associated RP include accumulation of misfolded RHO within the ER stress-triggered activation of the unfolded protein response (UPR), and increased ROS, all of which contribute to chronic inflammation[12,14]. RP is now widely recognized to involve not only photoreceptor dysfunction but also activation of retinal glia[56]. Müller glia undergo reactive gliosis, marked by somatic hypertrophy, enhanced motility, and increased expression of

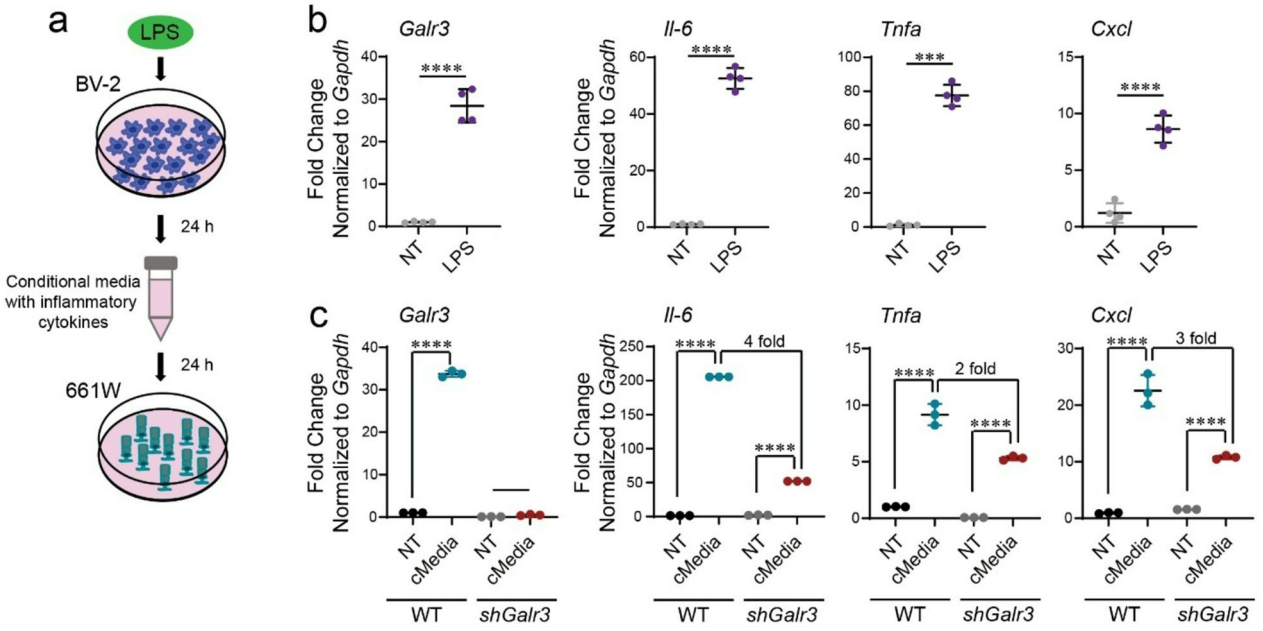


**Fig. 9**. Effects of GALR3 inhibition on photoreceptor cells exposed to microglia-mediated neurotoxicity in vitro. **a** Schematic of experimental design. BV-2 microglial cells were stimulated with LPS (1 µg/ml) for 24 h to induce an immune response. Conditioned media (cMedia) from LPS-treated BV-2 cells were collected and applied to photoreceptor-derived 661 W cells and *Galr3*-silenced 661 W cells (*shGalr3*) to assess secondary inflammatory effects. **b** LPS stimulation in BV-2 cells induced overexpression of the *Galr3* receptor and significantly increased the expression of pro-inflammatory cytokines, supporting a role of GALR3 in microglial activation. **c** 661 W cells treated with LPS-conditioned media also showed upregulation of *Galr3* and pro-inflammatory cytokines. In contrast, *shGalr3* 661 W cells showed suppressed *Galr3* expression and attenuated inflammatory responses, suggesting a cell-autonomous contribution of *Galr3* to photoreceptor inflammation. Error bars represent S.D. Statistical analysis was performed with one-way ANOVA and post hoc Turkey's tests. Statistically significant changes are shown with asterisks. $^{*}P<0.05$; $^{**}P<0.01$; $^{***}P<0.001$; $^{****}P<0.0001$.

GFAP, while microglia migrate to the outer retina to clear dying photoreceptors[43,45]. Initially protective, this glial response becomes maladaptive under chronic stress conditions, such as oxidative damage or inherited mutations, leading to sustained inflammation and progressive tissue damage[2,56].

Supporting the role of GALR3 in this inflammatory process[40,67], previous studies have shown that galanin, the endogenous agonist of GALR3, enhances chemokine and cytokine production in activated macrophages, implicating GALR3 signaling in the amplification of pro-inflammatory responses[41]. Consistent with this, we found that both pharmacological inhibition and genetic ablation of GALR3 in *Rho*$^{P23H/+}$ mice markedly attenuated Müller cell gliosis and reduced the number of IBA-1-positive microglia. Inflammatory cytokines were also significantly decreased in the retinas of *Galr3*-deficient or GALR3-antagonist-treated mice. In addition, activation of NF-κB and inflammasome markers associated with pro-inflammatory cytokine release were diminished in treated mice, indicating that GALR3 promotes retinal degeneration by amplifying pro-inflammatory signaling. Conversely, blocking GALR3 not only suppressed these pathways but also elevated markers of anti-inflammatory signaling, highlighting its role in maintaining immune balance in the retina.

This persistent low-grade chronic inflammation in RP is likely driven by increased ROS stemming from reduced oxygen consumption in the outer retina due to photoreceptor loss[68,69]. Supporting this, treatment with antioxidants decreases photoreceptor degeneration in RP mouse models[26,68]. In this study, we found that oxidative stress defense pathways, particularly NRF2, a key transcription factor in redox homeostasis[70], were compromised in *Rho*$^{P23H/+}$ mice. Interestingly, the inhibition of GALR3 signaling led to the restoration of NRF2 expression and upregulation of downstream antioxidant enzymes, further linking GALR3 to oxidative stress regulation.

This interplay between oxidative stress and inflammation is consistent with findings in neuronal systems[71]. In hypothalamic neurons, ROS accumulation was shown to induce ER stress and Bax/Bcl-2-mediated apoptosis, while simultaneously upregulating GALR3 and spexin. These findings suggest that oxidative stress may activate the galanin-GALR3 axis, contributing to neuroinflammation and degeneration across neural tissues.

In addition to glial activation and inflammation, the BRB disruption is another hallmark of RP progression[30–32]. This disruption allows peripheral immune cells, including macrophages and neutrophils, to infiltrate the retina, where they become activated by factors released from dying photoreceptors and further amplify local inflammation[46,56]. Notably, increased levels of GALR3 were found in M1 proinflammatory macrophages[41]. In *Rho*$^{P23H/+}$ mice, we observed significant compromise of both the inner BRB and outer BRB, evidenced by reduced tight junction integrity among RPE cells and increased retinal capillary leakage. Importantly, GALR3 inhibition

restored BRB integrity, with improvements in tight junction structure and decreased albumin leakage. In both GALR3 antagonist-treated *Rho*$^{P23H/+}$ mice and *Rho*$^{P23H/+}$*Galr3*$^{-/-}$ mice, cell-cell contacts between RPE cells more closely resembled those of WT mice retinas. These findings identify GALR3 as a previously unrecognized regulator of BRB stability and further support its role in inflammation-associated vascular dysfunction in RP.

To further probe the role of GALR3 in inflammation-induced retinal toxicity, we employed an in vitro model using 661 W photoreceptor-derived cells. When exposed to conditioned media from LPS-activated BV-2 microglia, WT 661 W cells mounted a robust inflammatory response, characterized by elevated stress and inflammatory markers. In contrast, 661 W cells with silenced GALR3 were significantly more resistant to the same inflammatory insult. These findings strongly support the role of GALR3 in mediating microglia-induced photoreceptor toxicity and complement our in vivo data showing that GALR3 inhibition mitigates retinal inflammation and preserves BRB integrity.

Together, our findings establish GALR3 as a critical modulator of retinal inflammation, oxidative stress, and vascular integrity in RP. By promoting glial reactivity, inflammatory cytokine production, and BRB breakdown, GALR3 contributes to disease progression. Inhibiting GALR3 signaling, conversely, offers a multifaceted therapeutic strategy, suppressing inflammation, enhancing antioxidant defense, and stabilizing the neurovascular unit. Importantly, these effects are independent of the underlying genetic mutation, suggesting that GALR3 may serve as a promising mutation-agnostic target for treating RP and potentially other forms of retinal degeneration.

## Materials and methods

All methods used in this current study were performed in accordance with the relevant guidelines and regulations.

### Chemicals and reagents

Dimethylsulfoxide (DMSO) and EDTA-free protease inhibitor cocktail tablets were purchased from Sigma (St. Louis, MO). RIPA lysis buffer was obtained from Thermo Fisher Scientific (Pittsburg, PA). Peanut agglutinin (PNA) and Alexa Fluor 488-conjugated streptavidin were purchased from Vector Laboratories (Newark, CA). Polyvinylidene difluoride (PVDF) membrane was obtained from Millipore (Burlington, MA). The GALR3 antagonist SNAP-37,889 was purchased from Alomone Labs (Jerusalem, Israel) (PubChem CID 1471834). Fluoromount-G slide mounting medium purchased from SouthernBiotech (Birmingham, AL). GALR3 shRNA (m) Lentiviral Particles (sc-40011-V) were purchased from Santa Cruz Biotechnology, Inc. (Dallas, TX). All antibodies used in this study are listed in Table 1.

### Animals care

Homozygous *Rho*$^{P23H/P23H}$ mice (Research Resource Identifier, RRID:IMSR_JAX:017628) and *Galr3*$^{-/-}$ mice (RRID:IMSR_TAC: tf0230) (Taconic, Germantown, NY) were crossed to generate *Rho*$^{P23H/+}$*Galr3*$^{-/-}$ mice as described in Ortega et al.[33]. *Rho*$^{P23H/P23H}$ were crossed with WT C57BL/6J mice (RRID:IMSR_JAX:000664), (Jackson Laboratory, Bar Harbor, ME) to obtain heterozygous *Rho*$^{P23H/+}$ mice[16]. Both male and female mice were used in all experiments. All mice were housed in the Animal Resource Center at the School of Medicine, Case Western Reserve University (CWRU), and maintained in a 12-hour light/dark cycle. All the procedures involving mice and experimental protocols comply with the Animal Welfare Act guidelines and the ARRIVE guidelines and were approved by the Case Western Reserve University Institutional Animal Care and Use Committee

| Antibody Name | Species | Source | Identifiers | Dilution |
|---|---|---|---|---|
| Anti-M-Opsin | Rabbit polyclonal | Millipore | NP_064445 | 1:1000 |
| Anti-GFAP | Rabbit polyclonal | Thermo Fisher Scientific | PA1-9565 | 1:1000 |
| Anti-IBA-1 | Rabbit polyclonal | Thermo Fisher Scientific | PA5-27436 | 1:100 IHC |
| Anti-NLRP3 | Rabbit polyclonal | Cell Signaling | 15,101 S | 1:1000 |
| Anti-NFκB (p60) | Rabbit polyclonal | Proteintech | 10745-1-AP | 1:1000 |
| Anti-IκB | Rabbit polyclonal | Cell Signaling | 4812 S | 1:1000 |
| Anti-P-Iκb | Rabbit polyclonal | Cell Signaling | 2859 S | 1:1000 |
| Anti-Catalase | Rabbit polyclonal | Abclonal | A18018 | 1:1000 |
| Anti-Caspase-1 | Mouse monoclonal | Santa Cruz | sc-56,036 | 1:200–1:1000 |
| Anti-GCLc | Rabbit polyclonal | Invitrogen | PA5-103134 | 1:500 |
| Anti-Albumin FITC-conjugated | Rabbit polyclonal | Fortis Life Sciences | A90-234 F | 1:400 |
| Anti-GALR3 | Rabbit polyclonal | Thermo Fisher Scientific | PA5-19206 | 1:200 |
| Anti-GAPDH | Mouse monoclonal | Abclonal | AC002 | 1:10,000 |
| Anti-mouse IgG, HRP-conjugate | Goat | Promega | W4021 | 1:10,000 |
| Anti-rabbit IgG, HRP-conjugated | Goat | Promega | W4011 | 1:10,000 |
| Anti-mouse IgG Alexa Fluor 555-conjugated | Goat | Thermo Fisher Scientific | A28180 | 1:400 |
| Anti-rabbit IgG Alexa Fluor 555-conjugated | Goat | Thermo Fisher Scientific | A27039 | 1:400 |
| Anti-mouse IgG Alexa Fluor 488-conjugated | Goat | Thermo Fisher Scientific | A28175 | 1:400 |

**Table 1**. List of used commercial antibodies.

(IACUC), and conformed to recommendations of both the American Veterinary Medical Association Panel on Euthanasia and the Association for Research in Vision and Ophthalmology, as well as the National Eye Institute Animal Care and Use Committee (NEI-ASP 682). Efforts were taken to minimize animal suffering.

### Treatment of *Rho*$^{P23H/+}$ mice

We investigated the molecular mechanism of retina protection in *Rho*$^{P23H/+}$ mice with SNAP-37,889, the specific GALR3 antagonist[34]. *Rho*$^{P23H/+}$ mice were treated with SNAP-37,889 at 10 mg/kg b.w. every other day in the morning for 2 or 4 weeks. This compound was delivered to mice via intraperitoneal (i.p.) injection. Six or 12 injections in total were performed. Mice were analyzed at postnatal day 33 (P33) or P45 as described in[33,63,72,73]. The retinal morphology was assessed with SD-OCT ($n$ = 6 mice per group), and retinal function was examined with ERG ($n$ = 5 mice per group). Before each procedure, mice were anesthetized with a cocktail containing ketamine (20 mg/ml) and xylazine (1.75 mg/ml) at a dose of 4 µl/g b.w. For histological and immunohistochemical retinal analyses, eyes were collected from euthanized mice ($n$ = 6 per group).

### SD-OCT i*n vivo* retina imaging

The effect of pharmacological inhibition and genetic depletion of GALR3 on retina degeneration caused by P23H mutation in RHO was assessed using the ultrahigh-resolution Spectral-Domain Optical Coherence Tomography (SD-OCT) in vivo imaging (Bioptigen, Morrisville, NC). The a-scan/b-scan ratio was set at 1200 lines. The OCT images were obtained by scanning at 0 and 90 degrees in the b-mode. Five image frames were captured and averaged. Changes in the retina of treated and control mice were determined by measuring the thickness of the outer nuclear layer (ONL) at 0.5 mm from the optic nerve head (ONH). The following mouse strains were subjected to SD-OCT imaging: C57BL/6J, *Rho*$^{P23H/+}$, *Rho*$^{P23H/+}$ treated with GALR3 antagonist SNAP-37,889, and *Rho*$^{P23H/+}$*Galr3*$^{-/-}$. Six mice were used in each experimental group.

### Histological analysis

Eyes collected from euthanized mice were fixed in 0.5% glutaraldehyde in 2% paraformaldehyde (PFA) in PBS for 24 h at room temperature (RT) on a rocking platform. Next day, eyes were transferred to 1% PFA for 48 h at RT. These eyes embedded in paraffin were sectioned (5 µm thick sections) and stained with hematoxylin and eosin (H&E). A ZEISS Axio Scan.Z1 slide scanner (Carl Zeiss Microscopy GmBH, Jena, Germany) and Zeiss-Zen 3.2 software (blue edition) were used to scan and analyze the retina sections.

### Immunohistochemistry

Mouse eyes fixed in 2% PFA for 72 h at RT were used to prepare 8 µm-thick cryosections. Before immunolabeling, sections were blocked with 10% normal goat serum (NGS) and 0.3% Triton X-100 in PBS for 1 h at RT and then stained overnight at 4 °C with the primary antibody. The next day, sections were washed with PBS 3 times for 5 min. Then, they were incubated with the secondary antibody for 2 h at RT. Alexa Fluor 555-conjugated goat anti-mouse or anti-rabbit antibodies were used as secondary antibodies with a dilution of 1:400. The GFAP-positive Müller glia were detected with a rabbit polyclonal anti-GFAP antibody at a 1:200 dilution. The IBA-1-positive cells were detected with a rabbit polyclonal anti-IBA-1 antibody at a 1:100 dilution. The expression of NF-kB was detected with a rabbit polyclonal antibody at a 1:100 dilution. The expression of NLRP3 was detected with a mouse monoclonal antibody at a 1:100 dilution. More detailed information about antibodies used in this study is included in Table 1. Cell nuclei were detected by staining with DAPI. Slides were coverslipped with Fluoromount-G (SouthernBiotech).

### ERG

Scotopic and photopic ERG responses were recorded for both eyes of each mouse using a Celeris rodent ERG system and Espion Dyagnosys software Version 6 (Dyagnosys, LLC, Lowell, MA). The following mouse strains at P33 or P45 were subjected to ERG measurements: C57BL/6J, *Rho*$^{P23H/+}$, *Rho*$^{P23H/+}$ treated with SNAP-37,889, and *Rho*$^{P23H/+}$*Galr3*$^{-/-}$. Five mice were used in each experimental group. The ERG data were processed for each experimental group and presented as mean and standard deviation (S.D.) for both a-wave and b-wave amplitudes.

### Immunoblotting

The proteins were extracted from the whole mouse eyes. The eyes were mechanically homogenized in a RIPA lysis buffer (Thermo Fisher Scientific) containing a protease inhibitor cocktail (Sigma), followed by 30 min incubation at 4 °C. The lysates were centrifuged at 12,000$g$ for 15 min at 4 °C. The protein concentration was measured with a BCA Protein Assay Kit (Thermo Fisher Scientific) with bovine serum albumin as a standard. The protein samples (50 µg/lane) were separated with 10% or 12% SDS-PAGE gel electrophoresis and then transferred to a polyvinylidene difluoride (PVDF) membrane (Millipore). The PVDF membrane was blocked with 5% milk for 1 h at RT, and then incubated with the primary antibodies overnight, followed by horseradish peroxidase (HRP)-conjugated anti-mouse or anti-rabbit secondary antibody listed in Table 1. The immunoblots were developed with a ProSignal reagents kit and the Odyssey Imaging System (LI-COR, Biosciences). GAPDH was used as the loading control.

## Retinal flat mount

Mouse eyes were enucleated, fixed in PBS-buffered 4% paraformaldehyde solution, and stored at 4 °C until use. For better fixation, a window cut was made in the sclera. Under a dissection microscope, the muscles and connective tissues were removed from the eyeball. The anterior segments of the eye, including the cornea, iris, and lens, were carefully removed. Then, the eyecup was cut into four quadrants from the periphery to the optic nerve head, and retinal flat mounts were prepared. To obtain an RPE-choroid flat mount, the retina was carefully removed. To immune stain the flat mounts, tissue was washed thoroughly in PBS and kept in PBS for 24 h at 4 °C. Next, it was blocked with a mixture of 5% NGS and 5% BSA dissolved in PBS containing 0.5% Triton-X100 and 0.05% Tween 20 (PBST) for 24 h at 4 °C. Next, to detect tight junctions, eyecup was incubated with the primary polyclonal anti-ZO-1 antibody at a1:200 dilution overnight at 4 °C, and to detect albumin, retinal tissue, was incubated with the polyclonal anti-albumin antibody conjugated with FITC at a 1:100 dilution. The following day, the tissue was washed 4 times in PBS for 30 min at RT, and then eyecups were incubated with a secondary antibody (anti-rabbit Alexa Fluor 488-conjugated) at a 1:400 dilution for 3 h at RT. Alternatively, the incubation with the secondary antibody was performed overnight at 4 °C. The primary and secondary antibodies were dissolved in 1% NGS in PBST. Next, the tissue was washed with PBS for 30 min at RT, followed by incubation with DAPI for 30 min at RT. After that, the tissue was washed with PBS 4 times for 15 min at RT. The flat mount was then mounted in Fluoromount-G slide mounting medium and imaged using a fluorescent microscope.

## Cell culture

The 661 W cells, murine photoreceptor-derived cells, were generously provided by Dr. Muayyad Al-Ubaidi, University of Houston. These cells were cultured according to the instructions provided in DMEM supplemented with 10% FBS (Hyclone, Logan, UT), 0.04 mg/ml progesterone, 0.04 mg/ml hydrocortisone, 0.032 mg/ml putrescine, 0.04% β-mercaptoethanol, and 1 unit/ml penicillin with 1 µg/ml streptomycin (Life Technologies) at 37 °C under 5% $CO_2$.

The 661 W cells with silenced GALR3 were prepared using GALR3 shRNA (m) Lentiviral Particles (sc-40011-V) (Santa Cruz Biotechnology, Inc.) according to the manufacturer's protocol.

## RT-qPCR

The selected gene expression analysis was carried out in mouse eyes or retinas collected from $n = 6$ mice per treatment group. Total RNA was isolated using the Qiagen RNeasy Miniprep Kit following the manufacturer's protocol. Then, the samples were treated with DNase I, and RNA concentration was determined using a nanodrop spectrophotometer (Thermo Fisher Scientific). The RNA served as a template to obtain cDNA by using the QuantiTect Reverse Transcription Kit (Qiagen) following the manufacturer's protocol. Quantitative RT-qPCR amplification was performed using LUNA NEB SYBR Green Master Mix (NEB) using the StepOnePlus Real-Time PCR system (Applied Biosystems). The PCR conditions were as follows: 95 °C for 3 min followed by 40 cycles of 95 °C for 20 s and 60 °C for 60 s. Fluorescence data were acquired at a step of 60 °C, and a Melt curve step was added. *Gapdh* was used as a control housekeeping gene. All data were normalized to the *Gapdh* expression level, and the fold change was calculated for each gene. The $C_t$ values were obtained from the amplification curve analysis using StepOne software version 2.3. The gene expression was measured using the comparative $2^{-(\Delta\Delta Ct)}$ method. All primers used in this study are listed in Table 2.

## Statistical analyses

Immunoblots were performed at least 3 times, and protein bands were quantified using ImageJ software. Each assay included positive and negative controls. The data obtained from these analyses were shown as an average and standard deviation (S.D). For multiple comparisons, one or two-way ANOVA with Turkey's post hoc tests were used. For two groups comparison, the Student's t-test was used. All statistical calculations were performed using the Prism GraphPad 10 software. Type 1 error tolerance for the experiments was established at 5%. Values of $P < 0.05$ were considered statistically significant. Distinct personnel carried out the collection of data and its statistical analysis.

| Target | Species | Forward primer sequence 3'→5' | Reverse primer sequence 3'→5' |
|---|---|---|---|
| *Rhodopsin* | mouse | CTTCCTGATCTGCTGGCTTC | ACAGTCTCTGGCCAGGCTTA |
| *M-opsin* | mouse | GAGATTCAAGAAGCTGCGCC | TGTCCAGAACGAGTAGCC |
| *Nlrp3* | mouse | AAGCAATGCCCTTGGAGACA | CATTGTTGCCCAGGTTCAGC |
| *Ccl2* | mouse | TCTCCAGCCTACTCATTGGG | AGGTCCTGTCATGCTTCTG |
| *Cxcl* | mouse | CTTCCCTATGGCCCTCATC | AAGTGCTGCCGTCATTTTCT |
| *Il-6* | mouse | CAACGATGATGCACTTGCAGA | GTGACTCCAGCTTATCTCTTGGT |
| *Il-10* | mouse | AGGCGCTGTCATCGATTTCT | TGTTACACTCGCCCCCTTTG |
| *Il-18* | mouse | TTACAAGCATCCAGGCACAG | GAAGGTTTGAGGCGGCTTTC |
| *Tnfa* | mouse | GGTCTGGGCCATAGAACTGA | CAGCCTCTTCTCATTCCTGC |
| *n-nos synthase* | mouse | GTGCTGGAAGTACCCATCAG | GGGAGGCCATACCATTTGAG |
| *Tgfb1* | mouse | CGTGGAAATCAACGGGATCA | TAGTTGGTATCCAGGGCTCTC |
| *Collagen-1A1* | mouse | TTACAGGGTAACGTTGGTGC | ACGGTCACCCTGGGAAC |
| *Pparg* | mouse | GTGGGGATGTCTCACAATGG | AAAGATGGGAGCTGGGTGTA |
| *Gpx4* | mouse | CCGTCTGAGCCGCTTACTTA | TATCGGGCATGCAGATCGAC |
| *Catalase* | mouse | ACCACACATCCTGAACGAGGAG | GATGAAGCAGTGGAAGGAGC |
| *Hmox-1* | mouse | TCAAGGCCTCAGACAAATCC | ACAACCAGTGAGTGGAGCCT |
| *Sod1* | mouse | AAAATGAGGTCCTGCACTGG | ACCATCCACTTCGAGCAGAA |
| *Sod2* | mouse | GCTTGATAGCCTCCAGCAAC | AACTCAGGTCGCTCTTCAGC |
| *Nfκb* | mouse | CCCTACGGAACTGGGCAAAT | CAAATCTGTTGCAAGGGGC |
| *Nrf2* | mouse | ATCTCCTAGTTCTCCGCTGC | CAAAACTTGTACCGCCTCGT |
| *Caspase-1* | mouse | AGTCCTGGAAATGTGCCATC | TACCTGGCAGGAATTCTGGA |
| *Gapdh* | mouse | TTGAGGTCAATGAAGGGGTC | TCGTCCCGTAGACAAAATGG |
| *Galr3* | mouse | TCGTGTGCAAGACGGTACA | ACCGCCAGGTACCTATCCA |
| *Spexin* | mouse | CGCCTCCAGAAAGACGAAAC | AATTCCCTCCTTCATCTGCACC |

**Table 2**. List of used primers.

## Data availability

The data that support the findings of this study are included in the manuscript.

Received: 26 September 2025; Accepted: 29 January 2026
Published online: 07 February 2026

## References

1. Jastrzebska, B. & GPCR G protein complexes–the fundamental signaling assembly. *Amino Acids*. **45**, 1303–1314. https://doi.org/10.1007/s00726-013-1593-y (2013).
2. Wong-Riley, M. T. Energy metabolism of the visual system. *Eye Brain*. **2**, 99–116. https://doi.org/10.2147/EB.S9078 (2010).
3. Figueroa, A. G. & McKay, B. S. A G-Protein coupled receptor and macular degeneration. *Cells*. https://doi.org/10.3390/cells9040910 (2020).
4. Chang, Q., Chen, S. & Yang, T. The GPCR antagonistic drug CM-20 stimulates mitochondrial activity in human RPE cells. *Open. Biochem. J.* https://doi.org/10.2174/1874091X-v16-e2206270 (2022).
5. Saddala, M. S. et al. Data mining and network analysis reveals C-X-C chemokine receptor type 5 is involved in the pathophysiology of age-related macular degeneration. *J. Biomol. Struct. Dyn.* https://doi.org/10.1080/07391102.2021.1949391 (2021).
6. Figueroa, A. G. & McKay, B. S. GPR143 signaling and retinal degeneration. *Adv. Exp. Med. Biol.* **1185**, 15–19. https://doi.org/10.1007/978-3-030-27378-1_3 (2019).
7. Schrodl, F. et al. Distribution of Galanin receptors in the human eye. *Exp. Eye Res.* **138**, 42–51. https://doi.org/10.1016/j.exer.2015.06.024 (2015).
8. Chen, Y. et al. Systems Pharmacology identifies drug targets for Stargardt disease-associated retinal degeneration. *J. Clin. Invest.* **123**, 5119–5134. https://doi.org/10.1172/JCI69076 (2013).
9. Filipek, S., Stenkamp, R. E., Teller, D. C. & Palczewski, K. G protein-coupled receptor rhodopsin: a prospectus. *Annu. Rev. Physiol.* **65**, 851–879. https://doi.org/10.1146/annurev.physiol.65.092101.142611 (2003).
10. Palczewski, K., Hofmann, K. P. & Baehr, W. Rhodopsin–advances and perspectives. *Vis. Res.* **46**, 4425–4426. https://doi.org/10.1016/j.visres.2006.10.009 (2006).
11. Athanasiou, D. et al. The role of the ER stress-response protein PERK in rhodopsin retinitis pigmentosa. *Hum. Mol. Genet.* **26**, 4896–4905. https://doi.org/10.1093/hmg/ddx370 (2017).
12. Azam, M. & Jastrzebska, B. Mechanisms of rhodopsin-related inherited retinal degeneration and pharmacological treatment strategies. *Cells*. https://doi.org/10.3390/cells14010049 (2025).
13. Hartong, D. T., Berson, E. L. & Dryja, T. P. Retinitis pigmentosa. *Lancet* **368**, 1795–1809. https://doi.org/10.1016/S0140-6736(06)69740-7 (2006).
14. Bighinati, A., Adani, E., Stanzani, A., D'Alessandro, S. & Marigo, V. Molecular mechanisms underlying inherited photoreceptor degeneration as targets for therapeutic intervention. *Front. Cell. Neurosci.* **18**, 1343544. https://doi.org/10.3389/fncel.2024.1343544 (2024).
15. Chiang, W. C. et al. Robust Endoplasmic Reticulum-Associated degradation of rhodopsin precedes retinal degeneration. *Mol. Neurobiol.* **52**, 679–695. https://doi.org/10.1007/s12035-014-8881-8 (2015).

16. Sakami, S. et al. Probing mechanisms of photoreceptor degeneration in a new mouse model of the common form of autosomal dominant retinitis pigmentosa due to P23H Opsin mutations. *J. Biol. Chem.* **286**, 10551–10567. https://doi.org/10.1074/jbc.M110.209759 (2011).
17. Hollingsworth, T. J. et al. Proinflammatory pathways are activated in the human Q344X rhodopsin Knock-In mouse model of retinitis pigmentosa. Biomolecules. https://doi.org/10.3390/biom11081163 (2021).
18. Nimmerjahn, A., Kirchhoff, F. & Helmchen, F. Resting microglial cells are highly dynamic surveillants of brain parenchyma in vivo. *Science* **308**, 1314–1318. https://doi.org/10.1126/science.1110647 (2005).
19. Reichenbach, A. & Bringmann, A. Glia of the human retina. *Glia* **68**, 768–796. https://doi.org/10.1002/glia.23727 (2020).
20. Liu, X., Jiang, N. & Zhou, W. Various energetic metabolism of microglia in response to different stimulations. *Molecules*. https://doi.org/10.3390/molecules28114501 (2023).
21. Newton, F. & Megaw, R. Mechanisms of photoreceptor death in retinitis pigmentosa. *Genes (Basel)*. https://doi.org/10.3390/genes11101120 (2020).
22. Xiong, Y. et al. N-methyl-N-nitrosourea induces retinal degeneration in the rat via the Inhibition of NF-kappaB activation. *Cell. Biochem. Funct.* **34**, 588–596. https://doi.org/10.1002/cbf.3232 (2016).
23. Viringipurampeer, I. A. et al. NLRP3 inflammasome activation drives bystander cone photoreceptor cell death in a P23H rhodopsin model of retinal degeneration. *Hum. Mol. Genet.* **25**, 1501–1516. https://doi.org/10.1093/hmg/ddw029 (2016).
24. Kelley, N., Jeltema, D., Duan, Y. & He, Y. The NLRP3 inflammasome: an overview of mechanisms of activation and regulation. *Int. J. Mol. Sci.* https://doi.org/10.3390/ijms20133328 (2019).
25. Wang, K. et al. Retinal structure and function preservation by polysaccharides of wolfberry in a mouse model of retinal degeneration. *Sci. Rep.* **4**, 7601. https://doi.org/10.1038/srep07601 (2014).
26. Lee, S. Y. et al. N-Acetylcysteine promotes long-term survival of cones in a model of retinitis pigmentosa. *J. Cell. Physiol.* **226**, 1843–1849. https://doi.org/10.1002/jcp.22508 (2011).
27. Hu, C. et al. Inhibiting HMGB1/AGER/NF-kappaB pathway prevents pro-inflammatory microglia polarization and protect photoreceptors in retinitis pigmentosa. *Int. Immunopharmacol.* **149**, 114192. https://doi.org/10.1016/j.intimp.2025.114192 (2025).
28. Wooff, Y. et al. Caspase-1-dependent inflammasomes mediate photoreceptor cell death in photo-oxidative damage-induced retinal degeneration. *Sci. Rep.* **10**, 2263. https://doi.org/10.1038/s41598-020-58849-z (2020).
29. Zhang, Z. et al. NLRP3 deficiency attenuates secondary degeneration of visual cortical neurons following optic nerve injury. *Neurosci. Bull.* **36**, 277–288. https://doi.org/10.1007/s12264-019-00445-x (2020).
30. Diaz-Coranguez, M., Ramos, C. & Antonetti, D. A. The inner blood-retinal barrier: cellular basis and development. *Vis. Res.* **139**, 123–137. https://doi.org/10.1016/j.visres.2017.05.009 (2017).
31. Newsome, D. A. Retinal fluorescein leakage in retinitis pigmentosa. *Am. J. Ophthalmol.* **101**, 354–360. https://doi.org/10.1016/0002-9394(86)90831-7 (1986).
32. Larsen, M., Engler, C. B., Haim, M. & Lund-Andersen, H. Blood-retina barrier permeability is independent of trace substance lipid solubility in retinitis pigmentosa and in the healthy eye. *Int. Ophthalmol.* **21**, 229–234. https://doi.org/10.1023/a:1006044107353 (1997).
33. Ortega, J. T., Parmar, T. & Jastrzebska, B. Galanin receptor 3 - A new Pharmacological target in retina degeneration. *Pharmacol. Res.* **188**, 106675. https://doi.org/10.1016/j.phrs.2023.106675 (2023).
34. Swanson, C. J. et al. Anxiolytic- and antidepressant-like profiles of the galanin-3 receptor (Gal3) antagonists SNAP 37889 and SNAP 398299. *Proc. Natl. Acad. Sci. U S A.* **102**, 17489–17494. https://doi.org/10.1073/pnas.0508970102 (2005).
35. Kaser-Eichberger, A. et al. Distribution of the neuro-regulatory peptide Galanin in the human eye. *Neuropeptides* **64**, 85–93. https://doi.org/10.1016/j.npep.2016.11.007 (2017).
36. Porzionato, A. et al. Spexin expression in normal rat tissues. *J. Histochem. Cytochem.* **58**, 825–837. https://doi.org/10.1369/jhc.2010.956300 (2010).
37. Crawley, J. N. Galanin impairs cognitive abilities in rodents: relevance to alzheimer's disease. *Exp. Suppl.* **102**, 133–141. https://doi.org/10.1007/978-3-0346-0228-0_10 (2010).
38. Falkenstetter, S. et al. Galanin system in human glioma and pituitary adenoma. *Front. Endocrinol. (Lausanne)*. **11**, 155. https://doi.org/10.3389/fendo.2020.00155 (2020).
39. Botz, B. et al. Lack of Galanin 3 receptor aggravates murine autoimmune arthritis. *J. Mol. Neurosci.* **59**, 260–269. https://doi.org/10.1007/s12031-016-0732-9 (2016).
40. Locker, F. et al. Lack of Galanin receptor 3 alleviates psoriasis by altering Vascularization, immune cell Infiltration, and cytokine expression. *J. Invest. Dermatol.* **138**, 199–207. https://doi.org/10.1016/j.jid.2017.08.015 (2018).
41. Koller, A. et al. Galanin is a potent modulator of cytokine and chemokine expression in human macrophages. *Sci. Rep.* **9**, 7237. https://doi.org/10.1038/s41598-019-43704-7 (2019).
42. Pasquale, R. L., Guo, Y., Umino, Y., Knox, B. & Solessio, E. Temporal contrast sensitivity increases despite photoreceptor degeneration in a mouse model of retinitis pigmentosa. *eNeuro*. https://doi.org/10.1523/ENEURO.0020-21.2021 (2021).
43. Jahnke, L., Zandi, S., Elhelbawi, A., Conedera, F. M. & Enzmann, V. Characterization of macroglia response during tissue repair in a Laser-Induced model of retinal degeneration. *Int. J. Mol. Sci.* https://doi.org/10.3390/ijms24119172 (2023).
44. Sakami, S., Imanishi, Y. & Palczewski, K. Muller glia phagocytose dead photoreceptor cells in a mouse model of retinal degenerative disease. *FASEB J.* **33**, 3680–3692. https://doi.org/10.1096/fj.201801662R (2019).
45. Chen, Y., Xia, Q., Zeng, Y., Zhang, Y. & Zhang, M. Regulations of retinal inflammation: focusing on Muller glia. *Front. Cell. Dev. Biol.* **10**, 898652. https://doi.org/10.3389/fcell.2022.898652 (2022).
46. Yang, P., Mustafi, D. & Pepple, K. L. Immunology of retinitis pigmentosa and gene therapy-associated uveitis. *Cold Spring Harb Perspect. Med.* https://doi.org/10.1101/cshperspect.a041305 (2024).
47. Bai, Q., Xue, M. & Yong, V. W. Microglia and macrophage phenotypes in intracerebral haemorrhage injury: therapeutic opportunities. *Brain* **143**, 1297–1314. https://doi.org/10.1093/brain/awz393 (2020).
48. Zhou, T. et al. Microglia polarization with M1/M2 phenotype changes in rd1 mouse model of retinal degeneration. *Front. Neuroanat.* **11**, 77. https://doi.org/10.3389/fnana.2017.00077 (2017).
49. Zou, Y. et al. Quercetin regulates microglia M1/M2 polarization and alleviates retinal inflammation via ERK/STAT3 pathway. *Inflammation* **47**, 1616–1633. https://doi.org/10.1007/s10753-024-01997-5 (2024).
50. Saha, S., Buttari, B., Panieri, E., Profumo, E. & Saso, L. An overview of Nrf2 signaling pathway and its role in inflammation. *Molecules*. https://doi.org/10.3390/molecules25225474 (2020).
51. Vomund, S., Schafer, A., Parnham, M. J., Brune, B. & von Knethen, A. Nrf2, the master regulator of anti-oxidative responses. *Int. J. Mol. Sci.* https://doi.org/10.3390/ijms18122772 (2017).
52. Singh, S., Nagalakshmi, D., Sharma, K. K. & Ravichandiran, V. Natural antioxidants for neuroinflammatory disorders and possible involvement of Nrf2 pathway: A review. *Heliyon* **7**, e06216. https://doi.org/10.1016/j.heliyon.2021.e06216 (2021).
53. Sparrow, J. R., Hicks, D. & Hamel, C. P. The retinal pigment epithelium in health and disease. *Curr. Mol. Med.* **10**, 802–823. https://doi.org/10.2174/156652410793937813 (2010).
54. Wang, W. et al. Metabolic deregulation of the Blood-Outer retinal barrier in retinitis pigmentosa. *Cell. Rep.* **28**, 1323–1334. https://doi.org/10.1016/j.celrep.2019.06.093 (2019). e1324.
55. Du, X., Butler, A. G. & Chen, H. Y. Cell-cell interaction in the pathogenesis of inherited retinal diseases. *Front. Cell. Dev. Biol.* **12**, 1332944. https://doi.org/10.3389/fcell.2024.1332944 (2024).

56. Rashid, K., Akhtar-Schaefer, I. & Langmann, T. Microglia in retinal degeneration. *Front. Immunol.* **10**, 1975. https://doi.org/10.3389/fimmu.2019.01975 (2019).
57. Vinores, S. A. et al. Localization of blood-retinal barrier breakdown in human pathologic specimens by immunohistochemical staining for albumin. *Lab. Invest.* **62**, 742–750 (1990).
58. Vinores, S. A. et al. Blood-retinal barrier breakdown in retinitis pigmentosa: light and electron microscopic immunolocalization. *Histol. Histopathol.* **10**, 913–923 (1995).
59. Anderson, P. J. et al. Glial and endothelial blood-retinal barrier responses to amyloid-beta in the neural retina of the rat. *Clin. Ophthalmol.* **2**, 801–816. https://doi.org/10.2147/opth.s3967 (2008).
60. Zhang, S. X. et al. Genetic difference in susceptibility to the blood-retina barrier breakdown in diabetes and oxygen-induced retinopathy. *Am. J. Pathol.* **166**, 313–321. https://doi.org/10.1016/S0002-9440(10)62255-9 (2005).
61. Davies, L. C., Jenkins, S. J., Allen, J. E. & Taylor, P. R. Tissue-resident macrophages. *Nat. Immunol.* **14**, 986–995. https://doi.org/10.1038/ni.2705 (2013).
62. Ortega, J. T. & Jastrzebska, B. Neuroinflammation as a therapeutic target in retinitis pigmentosa and Quercetin as its potential modulator. *Pharmaceutics*. https://doi.org/10.3390/pharmaceutics13111935 (2021).
63. Ortega, J. T., Parmar, T., Carmena-Bargueno, M., Perez-Sanchez, H. & Jastrzebska, B. Flavonoids improve the stability and function of P23H rhodopsin slowing down the progression of retinitis pigmentosa in mice. *J. Neurosci. Res.* **100**, 1063–1083. https://doi.org/10.1002/jnr.25021 (2022).
64. Ortega, J. T., Parmar, T., Golczak, M. & Jastrzebska, B. Protective effects of flavonoids in acute models of Light-Induced retinal degeneration. *Mol. Pharmacol.* **99**, 60–77. https://doi.org/10.1124/molpharm.120.000072 (2021).
65. Gao, S. et al. Protective effect of a locked retinal chromophore analog against Light-Induced retinal degeneration. *Mol. Pharmacol.* **94**, 1132–1144. https://doi.org/10.1124/mol.118.112581 (2018).
66. Pashandi, Z. et al. Therapeutic potential of partial retinoid agonists against vertebrate rhodopsin misfolding disorders. *ACS Omega*. **10**, 57487–57502. https://doi.org/10.1021/acsomega.5c08072 (2025).
67. Barreto, S. G. et al. Galanin receptor 3–a potential target for acute pancreatitis therapy. *Neurogastroenterol Motil.* **23**, e141–151. https://doi.org/10.1111/j.1365-2982.2010.01662.x (2011).
68. Komeima, K., Rogers, B. S. & Campochiaro, P. A. Antioxidants slow photoreceptor cell death in mouse models of retinitis pigmentosa. *J. Cell. Physiol.* **213**, 809–815. https://doi.org/10.1002/jcp.21152 (2007).
69. Sanchez-Vallejo, V. et al. Alterations in glutamate cysteine ligase content in the retina of two retinitis pigmentosa animal models. *Free Radic Biol. Med.* **96**, 245–254. https://doi.org/10.1016/j.freeradbiomed.2016.04.195 (2016).
70. Ryu, J. et al. Nutrigenetic reprogramming of oxidative stress. *Taiwan. J. Ophthalmol.* **11**, 207–215. https://doi.org/10.4103/tjo.tjo_421 (2021).
71. Tran, A., Loganathan, N., McIlwraith, E. K. & Belsham, D. D. Palmitate and nitric oxide regulate the expression of Spexin and Galanin receptors 2 and 3 in hypothalamic neurons. *Neuroscience* **447**, 41–52. https://doi.org/10.1016/j.neuroscience.2019.10.028 (2020).
72. Ortega, J. T. et al. Chromenone derivatives as novel Pharmacological chaperones for retinitis pigmentosa-linked rod Opsin mutants. *Hum. Mol. Genet.* **31**, 3439–3457. https://doi.org/10.1093/hmg/ddac125 (2022).
73. Ortega, J. T. et al. Discovery of non-retinoid compounds that suppress the pathogenic effects of misfolded rhodopsin in a mouse model of retinitis pigmentosa. *PLoS Biol.* **23**, e3002932. https://doi.org/10.1371/journal.pbio.3002932 (2025).


## Acknowledgements

The authors thank Mrs. Catherine Doller and Mrs. Dawn Smith for technical support with preparation of H&E-stained and retinal cryosections. We also thank Mrs. Maryanne Pendergast for technical support with using the fluorescence microscope.

## Author contributions

Participated in research design: B.J. and M.A. Conducted experiments: M.A., Z.P., M.L., and BJ. Performed data analysis: M.A., Z.P., M.L., and B.J. Wrote or contributed to the writing of the manuscript: B.J., M.A., Z.P., and M.L.

## Funding

This research was supported by the National Institutes of Health (NIH) (R01EY032874 to B.J.) and the Visual Sciences Research Center Core Facilities at Case supported by NIH grant P30 core grant (P30EY011373). This research also was in part supported by the Cleveland Clinic Foundations Cole Eye Institute T32 (5T32EY024236-09) and Molecular Pharmacology Training Program T32 (1T32GM158814-01) granted to the graduate student Mingda Liu.

## Declarations

## Competing interests

The authors declare no competing interests.

## Additional information

**Supplementary Information** The online version contains supplementary material available at https://doi.org/10.1038/s41598-026-38345-6.

**Correspondence** and requests for materials should be addressed to B.J.